

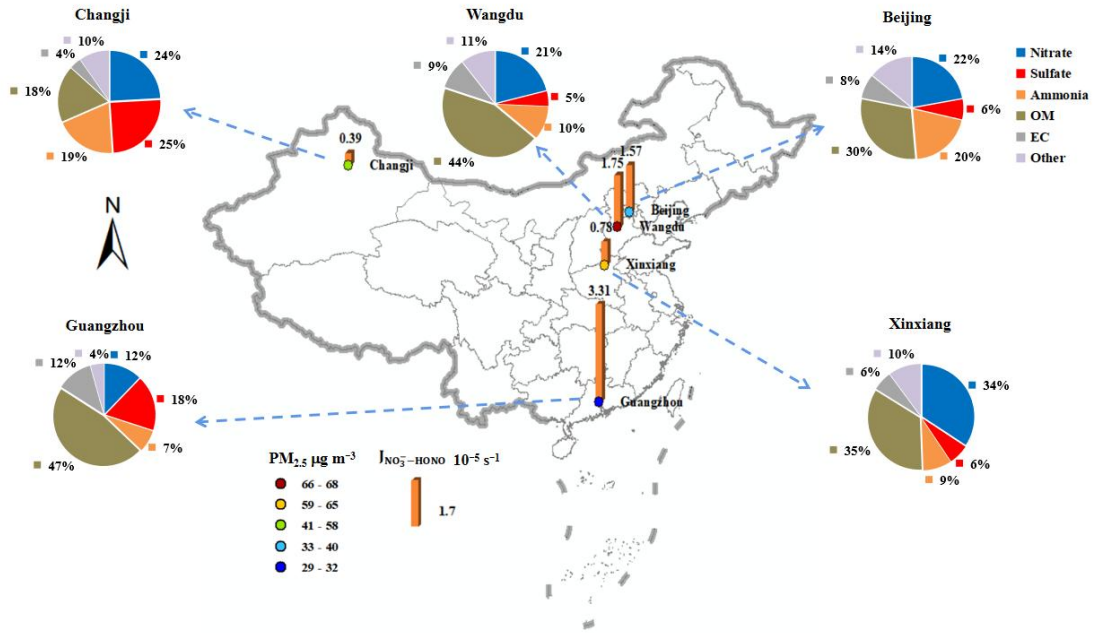
# Exploring HONO production from particulate nitrate photolysis in Chinese representative regions: characteristics, influencing factors and environmental implications

Bowen Li<sup>1</sup>, Jian Gao<sup>1</sup>, Chun Chen<sup>1</sup>, Liang Wen<sup>1</sup>, Yuechong Zhang<sup>1</sup>, Junling Li<sup>1</sup>, Yuzhe Zhang<sup>1</sup>, Xiaohui Du<sup>1</sup>, Kai Zhang<sup>1</sup>, Jiaqi Wang<sup>1</sup>

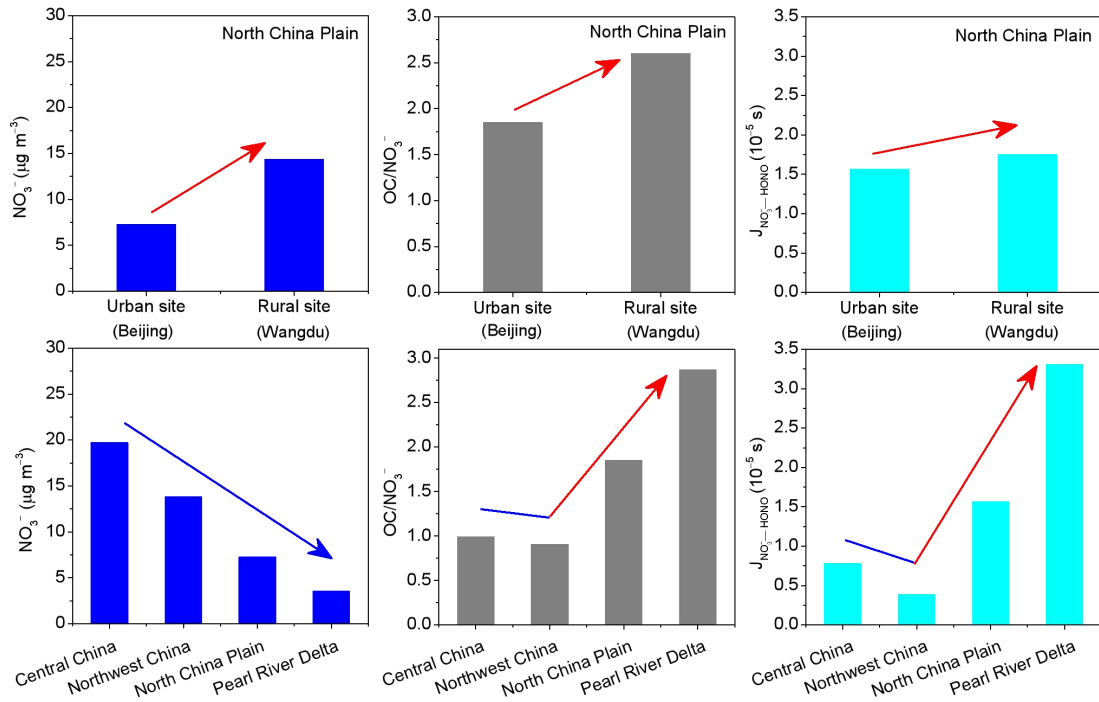
<sup>1</sup>State Key Laboratory of Environmental Criteria and Risk Assessment, Chinese Research Academy of Environmental Sciences, Beijing 100012, China

*Correspondence to:* Jiaqi Wang (wang.jiaqi@craes.org.cn), Kai Zhang (zhangkai@craes.org.cn)

**Abstract.** The production mechanism of atmospheric nitrous acid (HONO), an important precursor of hydroxyl radical (OH), was still controversial. Few studies have explored the effects of particulate nitrate photolysis on HONO sources in different environment conditions across China. In this work, the photolysis rate constants of particulate nitrate for HONO production ( $J_{\text{NO}_3^--\text{HONO}}$ ) were determined through photochemical reaction system with PM<sub>2.5</sub> samples collected from five representative sites in China. We developed a method to correct and quantify the “shadowing effect” — potential light extinction within aerosol layers at heavy PM<sub>2.5</sub> loadings on the filters — for  $J_{\text{NO}_3^--\text{HONO}}$  measurements, which showing that elemental carbon (EC), the dominant light-absorbing component in PM<sub>2.5</sub>, played a dominant role in it. The corrected  $J_{\text{NO}_3^--\text{HONO}}$  values varied with sampling period and location over a wide range, distributing from  $1.6 \times 10^{-6} \text{ s}^{-1}$  to  $1.96 \times 10^{-4} \text{ s}^{-1}$ , with a mean ( $\pm 1$  SD) of  $(1.71 \pm 2.36) \times 10^{-5} \text{ s}^{-1}$ . Chemical compositions, specifically nitrate loading and organic component, affected the production of HONO through particulate nitrate photolysis: high  $J_{\text{NO}_3^--\text{HONO}}$  values were generally associated with the PM<sub>2.5</sub> samples with high OC/NO<sub>3</sub><sup>-</sup> ratio ( $R^2=0.86$ ). We suggested that the parameterization equation between  $J_{\text{NO}_3^--\text{HONO}}$  and OC/NO<sub>3</sub><sup>-</sup> established in this work can be used to estimate  $J_{\text{NO}_3^--\text{HONO}}$  in different aerosol chemical conditions, thus reducing the uncertainty in exploring HONO daytime sources. This study confirms that the photolysis of particulate nitrate can be a potential HONO daytime source in rural or southern urban sites, which are characterized by high proportion of organic matter in PM<sub>2.5</sub>.



29



30

## 31 **1 Introduction**

32 Gaseous nitrous acid (HONO) is an important nitrogen-containing trace gas in the troposphere,  
33 which can produce hydroxyl radical (OH) through photolysis, thus stimulating the enhancement of  
34 atmospheric oxidation and the formation of secondary aerosols (Fu et al., 2019; Slater et al., 2020; Ren  
35 et al., 2003; Li et al., 2011; Su et al., 2011). In recent years, the contribution of HONO to atmospheric  
36 oxidation in heavily polluted conditions has attracted great attention (Villena et al., 2011; Fu et al.,  
37 2019; Slater et al., 2020). Even though observational research on HONO has been conducted for nearly  
38 40 years, the understanding of HONO daytime source was still controversial (Fu et al., 2019; Wang et  
39 al., 2017; Mora Garcia et al., 2021). Numerous mechanisms have been proposed to explain the  
40 extremely high HONO concentrations at noon, including direct combustion emission (Kurtenbach et al.,  
41 2001; Liang et al., 2017; Liao et al., 2021), gas-phase reaction of NO and OH radical (Li et al., 2011;  
42 Zhang et al., 2016), heterogeneous reaction of NO<sub>2</sub> (Wang et al., 2017; Ammann et al., 1998; Monge et  
43 al., 2010; Stemmler et al., 2006), soil emissions (Su et al., 2011; Oswald et al., 2013; Melissa A, 2014;  
44 Kim and Or, 2019), and the photolysis of HNO<sub>3</sub>/nitrate on aerosol or ground surface (Zhou et al., 2003;  
45 Zhou et al., 2011; Ye et al., 2016b; Ye et al., 2016a; Ye et al., 2017).

46 Particulate nitrate, which was conventionally considered as the ultimate oxidation product of NO<sub>x</sub>,  
47 can rapidly photolyze and recycle NO<sub>x</sub> or HONO back to the gas phase (Andersen et al., 2023; Handley  
48 et al., 2007; Beine et al., 2006; Ye et al., 2016a; Ye et al., 2017; Ye et al., 2016b; Gu et al., 2022b), at a  
49 rate 10 to 300 times faster than the photolysis rate of gaseous HNO<sub>3</sub> ( $\sim 7 \times 10^{-7} \text{ s}^{-1}$ ) under typical  
50 tropical noontime conditions (Finlayson-Pitts, 2000). Recently, some field, laboratory and modeling  
51 works have proposed that photolysis of particulate nitrate can be an important in situ source of HONO  
52 in rural, suburban and urban environments (Ye et al., 2016b; Mora Garcia et al., 2021; Liu et al., 2019;  
53 Bao et al., 2018; Wang et al., 2017). Fu et al. (2019) found that the photolysis of HNO<sub>3</sub>/nitrate in the  
54 atmosphere and deposited on surfaces was the dominant HONO source during noon and afternoon,  
55 contributing above 50 % of the simulated HONO. However, there are large discrepancies in estimating  
56 the rate constants in the atmosphere (Gen et al., 2022). In New York, Ye et al. (2017) reported that the  
57 photolysis rates of particulate nitrate in clean areas were two orders of magnitude higher than that in  
58 polluted areas, ranging from  $6.2 \times 10^{-6}$  to  $5.0 \times 10^{-4} \text{ s}^{-1}$ , with a median of  $8.3 \times 10^{-5} \text{ s}^{-1}$ . The proposed rate  
59 constants of nitrate photolysis based on the aircraft observations over South Korea ranged from  $7 \times 10^{-6}$

60 to  $2.1 \times 10^{-5} \text{ s}^{-1}$  (Romer et al., 2018). Shi et al. (2021) derived the rate constant ( $< 2 \times 10^{-5} \text{ s}^{-1}$ ) based on  
61 chamber experiments, but found a limited role of this mechanism to HONO production. The  
62 uncertainty of HONO production rate from the photolysis of particulate nitrate can reach up to 1.4 ppbv  
63  $\text{h}^{-1}$ , and greatly affect the accuracy of HONO source analysis (Liu et al., 2019; Lee et al., 2016; Ye et  
64 al., 2016a). The highly-varied photolysis rate constant of particulate nitrate was closely associated with  
65 environmental conditions and the aerosol chemical or physical characteristics, such as relative humidity  
66 (RH), aerosol acidity, light intensity, and coexisting components (organic components, halogen, etc.)  
67 (Gelencsér et al., 2003; Ye et al., 2016a; Bao et al., 2020; Wang et al., 2021; Reeser et al., 2013).  
68 Elucidating the mechanism and dominant factors controlling the photolysis of particulate nitrate is  
69 important to accurately estimate the HONO production rates from nitrate photolysis, thus improving  
70 estimations of HONO budgets.

71 In general, the photolysis rate constant of particulate nitrate was derived though photochemical  
72 experiments using bulk particle samples collected on filters (Ye et al., 2017; Bao et al., 2018).  
73 Comparing with the suspended particles in the ambient atmosphere, the collected  $\text{PM}_{2.5}$  particles in the  
74 aerosol filters may present a multiple-layer structure, especially in heavy air pollution conditions (Bao  
75 et al., 2018). The light-absorbing species within  $\text{PM}_{2.5}$  particles would hinder the light absorption of  
76 particulate nitrate in the lower layers of the filter sample, thus inhibiting the photolysis of particulate  
77 nitrate, which was called the “shadowing effect” (Ye et al., 2017). The shadowing effect of the aerosol  
78 filters collected in clean air conditions may be negligible, but this effect should be evaluated and  
79 quantified in heavy haze conditions where the aerosol loading was much heavier under the same  
80 sampling time. However, previous works generally ignored this shadowing effect.

81 According to previous field observations, the  $\text{PM}_{2.5}$  chemical composition, especially particulate  
82 nitrate ( $\text{NO}_3^-$ ), showed obvious spatial differences across China (Wang et al., 2022a, b; Wang et al.,  
83 2022c; Wang et al., 2016; Cheng et al., 2024). As one of the key industrial development areas in China,  
84 the Pearl River Delta Region (PRD) has a great number of large-scale industrial parks dominated by the  
85 chemical industry, resulting in significant VOC emissions and a large proportion of organic matter (OM)  
86 in  $\text{PM}_{2.5}$ . In the North China Plain (NCP), the particulate nitrate ( $\text{NO}_3^-$ ) has surpassed sulfate ( $\text{SO}_4^{2-}$ )  
87 and OM to become the dominant  $\text{PM}_{2.5}$  component in recent years (Wang et al., 2022b). For now, the  
88 investigation of particulate nitrate photolysis in different atmospheric environments was limited in  
89 China, and the influence of aerosol chemical or physical characteristics on HONO production was still

90 unclear. In this work, to shed light on the contribution of particulate nitrate photolysis to the HONO  
91 daytime source, we examined the photolysis rate constant for HONO based on photochemical  
92 experiments with PM<sub>2.5</sub> samples collected from five typical sites in China. In addition, the shadowing  
93 effect due to increasing aerosol particle loading on the filters was quantified. After correcting this effect,  
94 the influence of various environmental conditions, including particulate nitrate, organic matter, and  
95 aerosol acidity, on the formation of HONO was investigated and the possible role of this photolytic  
96 process as HONO sources was also examined.

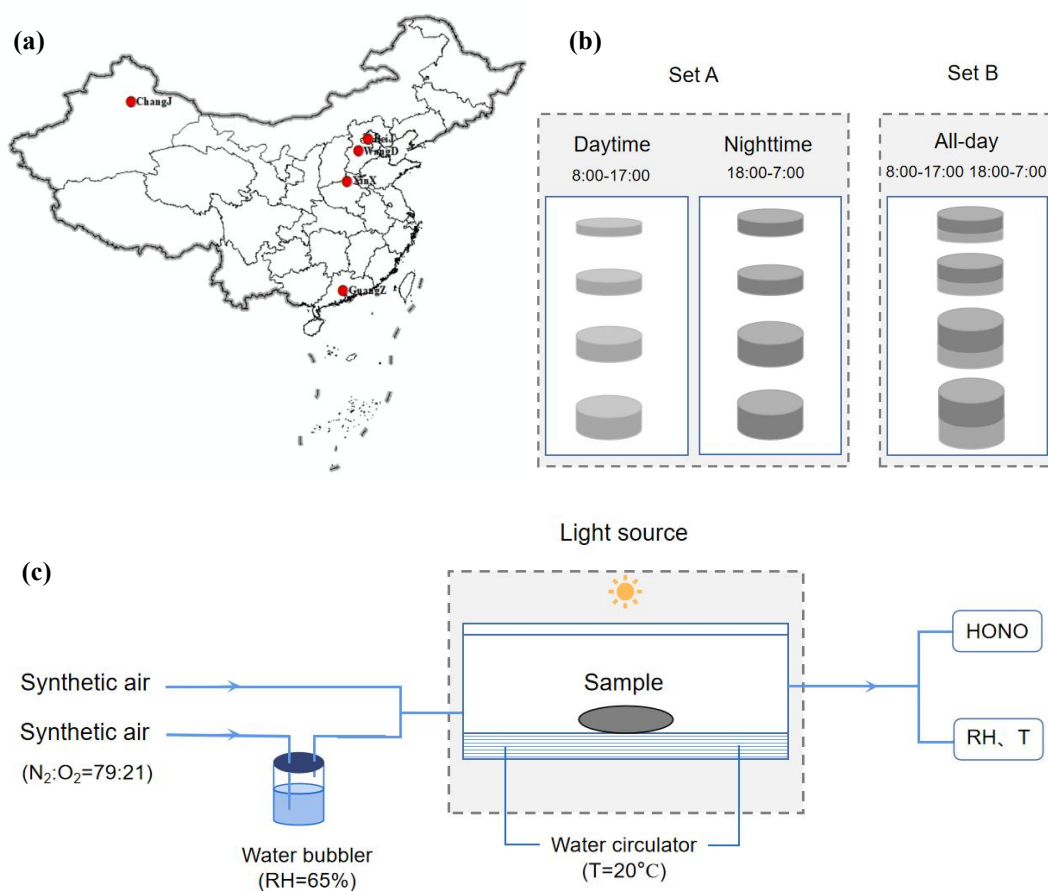
## 97 **2 Method**

### 98 **2.1 Sampling and filter treatment**

99 The ambient PM<sub>2.5</sub> was collected on Teflon or quartz filters in autumn-winter seasons in five  
100 representative sites, i.e., Beijing, Wangdu, Xinxiang, Guangzhou, and Changji, which were shown in  
101 Figure 1a and described in detail in the Supporting Information. These cities were located in the North  
102 China Plain (NCP, urban: Beijing, rural: Wangdu), Central China, Pearl River Delta Region (PRD), and  
103 Northwestern China, respectively. The sampling flow rates ranged from 16.7 to 1050 L min<sup>-1</sup>, the  
104 sampling times from 9 h to 23 h, and the overall sampling volumes of air from 8 m<sup>3</sup> to 1450 m<sup>3</sup>, to  
105 collect a very wide range of particulate nitrate loadings. The comparison experiments between Teflon  
106 and quartz filters have been conducted, and no significant differences in HONO production rates from  
107 particulate nitrate photolysis have been found ( $T < 0.01$ ). The sampling settings employed in Wangdu  
108 were designed to quantify the shadowing effect (Figure 1b). In Wangdu, PM<sub>2.5</sub> was collected at a flow  
109 rate of 16.7 L min<sup>-1</sup> with four channels (A, B, C, and D). A and B channels were set for  
110 daytime (8:00–17:00) and nighttime (18:00–7:00) PM<sub>2.5</sub> samples, respectively, and the other two  
111 channels were for the “all-day” (including 8:00–17:00 and 18:00–7:00) PM<sub>2.5</sub> samples. A total of 158  
112 effective PM<sub>2.5</sub> samples were obtained in this study. These aerosol filter samples were labeled and  
113 stored at -20°C in the freezer.

114 Fractions with given surface area from each filter sample were used to perform photochemical  
115 reaction experiments and analysis of aerosol chemical components. For each PM<sub>2.5</sub> sample, the fraction  
116 with given surface area was rinsed by deionized water and then sonicated for 15 min. The amounts of  
117 water-soluble ions including Na<sup>+</sup>, NH<sub>4</sub><sup>+</sup>, K<sup>+</sup>, Mg<sup>2+</sup>, Ca<sup>2+</sup>, Cl<sup>-</sup>, NO<sub>3</sub><sup>-</sup>, and SO<sub>4</sub><sup>2-</sup> were measured by ion

118 chromatography (IC, Thermo ICS-2100). To measure the values of carbon components, including  
 119 organic carbon (OC) and elemental carbon (EC), a part ( $0.5024 \text{ cm}^2$ ) of each filter was detected using a  
 120 thermal optical carbon analyzer (DRI model 2015). The concentration of OM was obtained by  
 121 multiplying the OC concentration by a factor of 1.6 (Li et al., 2021).  $\text{PM}_{2.5}$  concentration was estimated  
 122 by the sum of all the water-soluble ions and carbon components. The surface concentration of  $\text{PM}_{2.5}$   
 123 and its components on aerosol filters were calculated through dividing the absorbed loading with the  
 124 geometric area of the aerosol filter sample ( $\mu\text{g cm}^{-2}$ ).



126  
 127 **Figure 1.** (a) Location map of five representative sampling sites in China, (b) the sampling settings to  
 128 quantify the shadowing effect in Wangdu, and (c) a schematic diagram of the photochemical  
 129 experimental setup.

## 130 2.2 Photochemical reaction system

131 A custom-made cylindrical quartz vessel was used as the photochemical flow reactor (Figure 1c).  
 132 The diameter was 10 cm and the depth was 2.5 cm, with a cell volume of  $\sim 200$  ml. A xenon lamp (300  
 133 W) was placed 20 cm above the reactor as the light source. The light was filtered by a Pyrex sleeve to

134 remove heat-generating infrared light. The effective light intensity in the center of the flow reactor,  
 135 where aerosol samples were placed, was measured to be about 0.5 times higher ( $1.5 \text{ kW m}^{-2}$ , measured  
 136 by a calibrated optical power meter) than that at tropical noon on the ground (solar elevation angle  
 137  $\theta=0^\circ$ ). Synthetic air, composed of ultrahigh-purity nitrogen and ultrahigh-purity oxygen mixed at a  
 138 ratio of 79:21, was used as the carrier gas. The relative humidity (RH) in the air flow was adjusted  
 139 through a water bubbler and monitored with an online RH sensor (Vaisala, HMT130). The aerosol filter  
 140 sample was exposed to the solar simulator radiation for 20 min. The photochemical reaction  
 141 experiment for each sample was repeated 2–3 times with different fractions from the same sample. The  
 142 gaseous product (i.e., HONO) released during the experiment was flushed out of the reactor by the  
 143 carrier gas and was detected online by a custom-built HONO analyzer, which had been applied in  
 144 several measurements previously (Zhang et al., 2020b; Li et al., 2021).

### 145 **2.3 HONO Production from the photolysis of particulate nitrate**

146 The production rates ( $\text{nmol h}^{-1}$ ) of HONO from particulate nitrate photolysis ( $P_{\text{HONO}}$ ) were  
 147 calculated from their time-integrated signals above the baselines over the period of light exposure:

$$148 \quad P_{\text{HONO}} = \frac{F_g \times 60}{V_m(t_2 - t_1)} \int_{t_1}^{t_2} C_{\text{HONO}} dt \quad (1)$$

149 Where  $F_g$  ( $\text{L min}^{-1}$ ) is the flow rate of the carrier gas,  $V_m$  ( $24.5 \text{ L mol}^{-1}$ ) is the molar volume of gas at  
 150  $25^\circ \text{C}$  and  $1 \text{ atm}$  of pressure;  $t_1$  and  $t_2$  (min) are the starting and ending time of the irradiation,  
 151 respectively;  $C_{\text{HONO}}$  (ppb) is the online measured concentration of HONO. With the flow rate of  $2.5 \text{ L}$   
 152  $\text{min}^{-1}$ , the residence time in the reaction system was around  $\sim 5 \text{ s}$ . The photolytic loss of HONO was  
 153 less than  $5\%$ , thus no correction was made in the calculation of HONO production.

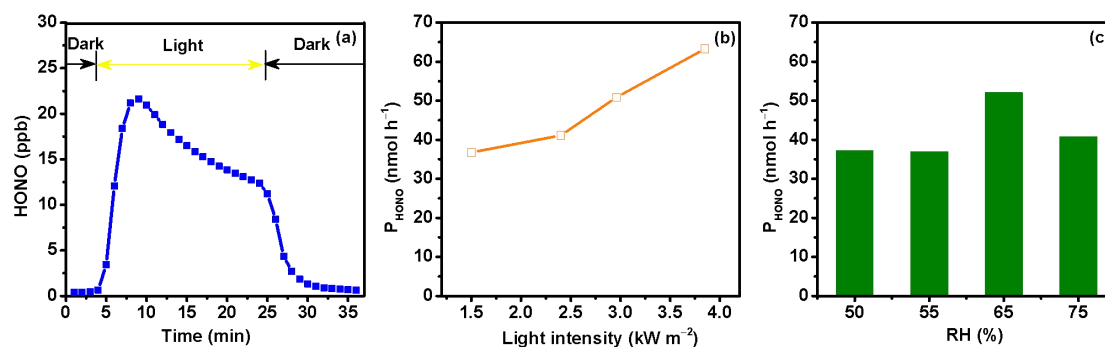
154 The photolysis rate constant of particulate nitrate leading to HONO production ( $J_{\text{NO}_3^- - \text{HONO}}$ ,  $\text{s}^{-1}$ )  
 155 was calculated by the following equation:

$$156 \quad J_{\text{NO}_3^- - \text{HONO}} = \frac{P_{\text{HONO}}}{N_{\text{NO}_3^-} \times 3600} \quad (2)$$

157 Where  $N_{\text{NO}_3^-}$  (mol) is the amount of  $\text{NO}_3^-$  in the tested  $\text{PM}_{2.5}$  sample. In principle, the photolysis rate  
 158 constant should be calculated on the amount of  $\text{NO}_3^-$  that is reachable to the irradiation. However, the  
 159 amount of the light-reachable  $\text{NO}_3^-$  in the  $\text{PM}_{2.5}$  sample was hard to quantify. In this work, the  
 160 deviation of  $J_{\text{NO}_3^- - \text{HONO}}$  due to the overestimate of the amount of  $\text{NO}_3^-$  under light irradiation, which  
 161 was called the shadowing effect, would be corrected in Sect. 3.1.

## 162 3 Results

### 163 3.1 Quantify the influence of the shadowing effect

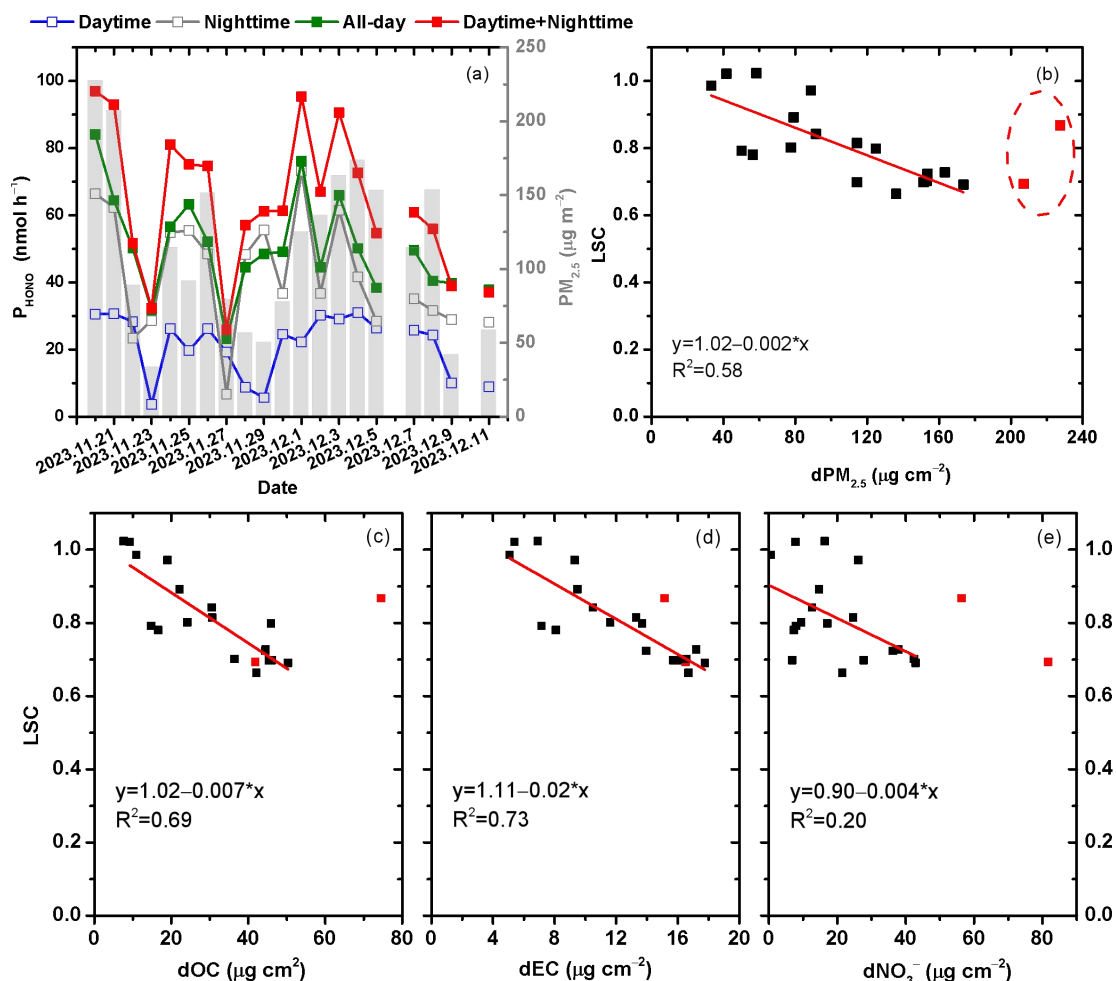


164

165 **Figure 2.** (a) Online measured concentrations of HONO during the light-exposure of an aerosol sample  
166 collected on June 12, 2023 in Beijing,  $P_{\text{HONO}}$  as a function of (b) light intensity ( $\text{kW m}^{-2}$ ) and (c) RH  
167 (%).

168 HONO production within the first 20 min of irradiation during the photochemical experiment was  
169 investigated on the  $\text{PM}_{2.5}$  samples collected from five typical sites in China. Figure 2a showed a typical  
170 profile of the changes in HONO concentration in the reaction system. When the light was turned on,  
171 HONO concentration in the reactor increased immediately, then leveled off and slightly decayed  
172 afterwards. After the light was turned off, the HONO generation stopped immediately and the signal  
173 nearly returned to the baseline level. Previous works have revealed that the decay of HONO generation  
174 during light exposure period was not resulted from the evaporation loss of particulate nitrate (Ye et al.,  
175 2017), but mainly related to the inhomogeneity of particulate nitrate photochemical reactivity or the  
176 consumption of reactive electron donors (Bao et al., 2018). HONO production from the photochemical  
177 reactions of particulate nitrate were significantly influenced by ambient environmental conditions (i.e.,  
178 light intensity and RH). As shown in Figure 2b, with the increase of light intensity,  $P_{\text{HONO}}$  gradually  
179 increased, with  $P_{\text{HONO}}$  in  $3.85 \text{ kW m}^{-2}$  approximately twice than that in  $1.50 \text{ kW m}^{-2}$ . Previous works  
180 found that the formation of HONO was negligible at low RH (<5%), and increased at intermediate RH  
181 (15%–75%), then turned to decrease at  $\text{RH} > 90\%$  (Bao et al., 2018). Here, we found that  $P_{\text{HONO}}$   
182 climbed to its highest when RH was around 65 % (Figure 2c). In this work, the photochemical  
183 reactions on different aerosol samples were all conducted under the same environmental condition  
184 (RH=65 %, temperature=20 °C, and light intensity=1.50  $\text{kW m}^{-2}$ ).





185

186

187 **Figure 3.** (a) Temporal variation of  $P_{\text{HONO}}$  for aerosol filters collected in Wangdu during daytime,  
 188 nighttime and all-day from November 20, 2023 to December 11, 2023, (b)-(e) relationships between  
 189 light screening coefficient (LSC) and the surface concentrations of  $\text{PM}_{2.5}$  ( $\text{dPM}_{2.5}$ ), OC (dOC), EC (dEC)  
 190 and  $\text{NO}_3^-$  ( $\text{dNO}_3^-$ ), respectively. The red squares represent the aerosol samples with  $\text{PM}_{2.5}$  surface  
 191 concentration higher than  $200 \mu\text{g cm}^{-2}$ .

192 As expected,  $P_{\text{HONO}}$  increased with particulate nitrate loadings in different sampling locations  
 193 (Figure S1), however, it's interesting to note that,  $P_{\text{HONO}}$  did not increase or somewhat decreased at very  
 194 high  $\text{NO}_3^-$  loading condition. This phenomenon has also been observed in other works (Ye et al., 2017;  
 195 Bao et al., 2018). Previous works considered this may be attributed to the shadowing effect of particles  
 196 at heavy aerosol loading on the filters. The particulate nitrate underneath the aerosol filters may receive  
 197 less UV light because of the presence of particles in the upper layers, inhibiting the photolysis of  
 198 particulate nitrate (Ye et al., 2017). Assuming that the sampling time of all aerosol filter samples was  
 199 the same, the aerosol loading on the filters collected under polluted conditions was much higher than  
 200 that under clean conditions. Thus, the reported  $P_{\text{HONO}}$  values for the aerosol filters collected under

201 polluted ambient conditions would be underestimated with heavy aerosol particle loading. To verify  
 202 and quantify the underestimation of  $P_{\text{HONO}}$  due to the shadowing effect, we collected two sets of filters  
 203 in Wangdu (set A: daytime and nighttime, set B: all-day, Figure 1b). Theoretically, the all-day one  
 204 should share the same  $\text{NO}_3^-$  loading and chemical composition as the sum of the daytime and nighttime  
 205 filters, thus the sum of  $P_{\text{HONO}}$  during daytime ( $P_{\text{daytime}}^{\text{HONO}}$ ) and nighttime ( $P_{\text{nighttime}}^{\text{HONO}}$ ) should be equal to that  
 206 during all-day ( $P_{\text{all-day}}^{\text{HONO}}$ ) without considering the shadowing effect. A total of 20 pairs of comparative  
 207 photochemical experiments were conducted, and the comparison of  $P_{\text{HONO}}$  between these two sets of  
 208 filters was shown in Figure 3a. We found that the discrepancy between  $P_{\text{all-day}}^{\text{HONO}}$  and  $P_{\text{daytime}}^{\text{HONO}} +$   
 209  $P_{\text{nighttime}}^{\text{HONO}}$  was widening along with the increase of surface  $\text{PM}_{2.5}$  concentration. To quantify the  
 210 shadowing effect, we introduced a parameter called “light screening coefficient” (LSC) to describe the  
 211 decreasing efficiency of light penetrating into the particle with increasing  $\text{PM}_{2.5}$  loadings:

$$212 \quad P_{\text{theory}}^{\text{HONO}} = P_{\text{daytime}}^{\text{HONO}} + P_{\text{nighttime}}^{\text{HONO}} \quad (3)$$

$$213 \quad \text{LSC} = P_{\text{observed}}^{\text{HONO}} / P_{\text{corrected}}^{\text{HONO}} = P_{\text{all-day}}^{\text{HONO}} / P_{\text{theory}}^{\text{HONO}} \quad (4)$$

214 where  $P_{\text{observed}}^{\text{HONO}}$  represented the observed production rate of HONO from particulate nitrate photolysis  
 215 through photochemical experiment, and  $P_{\text{corrected}}^{\text{HONO}}$  represented the corrected value of  $P_{\text{HONO}}$  after  
 216 quantifying the shadowing effect. As shown in Figure 3b, when  $\text{PM}_{2.5}$  surface concentration ( $\text{dPM}_{2.5}$ )  
 217 was low, LSC was almost equal to 1, indicating that the shadowing effect was negligible. With the  
 218 increase of  $\text{PM}_{2.5}$  loading, the value of LSC declined to lower than 65 %. In general, significant  
 219 negative correlation existed between LSC and  $\text{dPM}_{2.5}$ , except when  $\text{dPM}_{2.5}$  was higher than  $200 \mu\text{g cm}^{-2}$   
 220 (Figure 3b). In this experiment, we assumed that the daytime and nighttime  $\text{PM}_{2.5}$  samples were both  
 221 single-layered. However, with the increase of air pollution, these filters in each pair of comparative  
 222 experiments may already have exhibited the shadowing effect, thus the sum of  $P_{\text{daytime}}^{\text{HONO}}$  and  $P_{\text{nighttime}}^{\text{HONO}}$   
 223 would be underestimated. Therefore, when quantifying the shadowing effect, the LSC data with  $\text{PM}_{2.5}$   
 224 loading higher than  $200 \mu\text{g cm}^{-2}$  was excluded. Correlations between LSC and the surface  
 225 concentrations of  $\text{PM}_{2.5}$  major chemical components, such as EC (dEC), OC (dOC), and  $\text{NO}_3^-$  (d $\text{NO}_3^-$ ),  
 226 were conducted (Figure 3c-e). Significant correlation was found between LSC and carbonaceous  
 227 component, especially EC ( $R^2=0.73$ ), which was one of the most important light absorbing species in  
 228  $\text{PM}_{2.5}$ , indicating that the shadowing effect was mainly related to the light absorption components in  
 229  $\text{PM}_{2.5}$ . The relationship between LSC and dEC was established as following:

$$230 \quad \text{dEC} > 5.5 \mu\text{g m}^{-2}: \text{LSC} = 1.11 - 0.02 \times \text{dEC}$$

231  $dEC \leq 5.5 \mu\text{g m}^{-2}$ :  $LSC = 1$  (5)

232 when  $dEC \leq 5.5 \mu\text{g m}^{-2}$ , the shadowing effect can be ignored; when  $dEC > 5.5 \mu\text{g m}^{-2}$ ,  $P_{\text{HONO}}$  can be

233 corrected by the observed  $P_{\text{HONO}}$  and  $LSC$ , which was estimated using this fitting equation with  $dEC$ .

234 Previous works found that the heavy loads of carbonaceous particles can turn these filters into dark

235 brown colors. The UV light was unlikely to transmit efficiently through the dark layer to the particulate

236 nitrate underneath, thus inhibiting the generation of HONO from the photolysis of particulate nitrate

237 (Ye et al., 2017). In consideration of the potential shadowing effect for the daytime and nighttime filters

238 in each pair of comparative experiments, the  $P_{\text{daytime}}^{\text{HONO}}$  and  $P_{\text{nighttime}}^{\text{HONO}}$  observed would be

239 underestimated, and the uncertainty of  $LSC$  should be considered at high  $PM_{2.5}$  loadings. To evaluate

240 this uncertainty, the observed  $P_{\text{daytime}}^{\text{HONO}}$  and  $P_{\text{nighttime}}^{\text{HONO}}$  values were recalculated and corrected to the

241 theoretical single-layered condition based on Eq. (4) and (5). As shown in Figure S2, with the increase

242 of  $PM_{2.5}$  surface concentration, the deviations between  $LSC$  and the corrected one have enlarged.

243 However, it's noted that the deviation was still lower than 20 % when  $PM_{2.5}$  surface concentration was

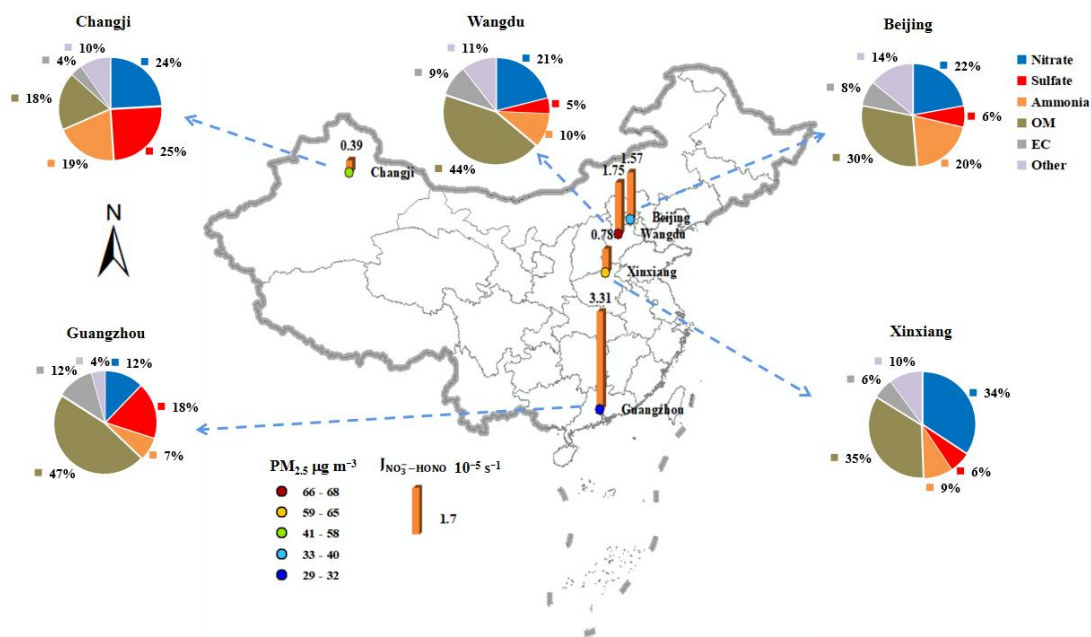
244 around  $200 \mu\text{g cm}^{-2}$ . For example, for the aerosol sample collected in December 4, 2023, in Wangdu,

245 the  $PM_{2.5}$  surface concentration was  $173.57 \mu\text{g cm}^{-2}$ , and the deviation was 15.74 %, which was

246 acceptable in this work.

### 247 3.2 Spatial distribution and temporal variation of HONO production from particulate nitrate

### 248 photolysis



249

250 **Figure 4.** Spatial distribution of the average ( $J_{\text{NO}_3\text{-HONO}}$ ,  $PM_{2.5}$  loading, and chemical composition of

251 the aerosol filters collected from five representative cities in China during the observation period.

252 There were 158 filter samples collected from five representative cities in China, and the averaged  
253 concentrations of PM<sub>2.5</sub> and its chemical composition of these filters showed significant spatial  
254 characteristics as shown in Figure 4. During the sampling period, OM was the most abundant species in  
255 PM<sub>2.5</sub> over most regions, except in the northwestern city (Changji), and NO<sub>3</sub><sup>-</sup> was the dominant  
256 inorganic component in the NCP (Beijing and Wangdu) and Central China (Xinxiang), while SO<sub>4</sub><sup>2-</sup>  
257 showed the highest contribution in the PRD (Guangzhou) and Northwestern China (Changji). The  
258 values of J<sub>NO<sub>3</sub><sup>-</sup>-HONO</sub> on these PM<sub>2.5</sub> samples were calculated by Eq. (2) with the P<sub>HONO</sub> corrected by  
259 Eq. (4) and (5), and summarized in Figure 4 and Table 1. The corrected J<sub>NO<sub>3</sub><sup>-</sup>-HONO</sub>, median and mean  
260 (± one standard deviation), were 1.55×10<sup>-5</sup> s<sup>-1</sup> and 1.57 (±2.14) ×10<sup>-5</sup> s<sup>-1</sup> in Beijing, 1.68×10<sup>-5</sup> s<sup>-1</sup> and  
261 1.75 (±2.83) ×10<sup>-5</sup> s<sup>-1</sup> in Wangdu, 0.69×10<sup>-5</sup> s<sup>-1</sup> and 0.78 (±0.48) ×10<sup>-5</sup> s<sup>-1</sup> in Xinxiang, 3.04×10<sup>-5</sup> s<sup>-1</sup>  
262 and 3.31 (±1.15) ×10<sup>-5</sup> s<sup>-1</sup> in Guangzhou, and 0.38×10<sup>-5</sup> s<sup>-1</sup> and 0.39 (±0.25) ×10<sup>-5</sup> s<sup>-1</sup> in Changji,  
263 respectively. The maximum J<sub>NO<sub>3</sub><sup>-</sup>-HONO</sub> in these cities ranged from 0.91×10<sup>-5</sup> s<sup>-1</sup> in Changji to  
264 1.96×10<sup>-4</sup> s<sup>-1</sup> in Wangdu. These values were in the comparable range to those previously reported for  
265 aerosol samples, such as 1.22×10<sup>-5</sup> s<sup>-1</sup>~ 4.84×10<sup>-4</sup> s<sup>-1</sup> in China by Bao et al. (2018) (RH = 60%,  
266 temperature = 25°C, irradiation time=15 min) and 6.2×10<sup>-6</sup> to 5.0×10<sup>-4</sup> s<sup>-1</sup> (the sum of HONO and  
267 NO<sub>x</sub> production, with an average HONO/NO<sub>x</sub> production ratio of ~2) in US by Ye et al. (2017) (RH =  
268 50%, temperature = 20(±1)°C, irradiation time=10 min). It's interesting to note that the average  
269 J<sub>NO<sub>3</sub><sup>-</sup>-HONO</sub> was the highest in Guangzhou, which was characterized with the lowest PM<sub>2.5</sub> and NO<sub>3</sub><sup>-</sup>  
270 concentration among these cities. As for other cities with high PM<sub>2.5</sub> concentrations, such as Changji  
271 and Xinxiang, the corrected J<sub>NO<sub>3</sub><sup>-</sup>-HONO</sub> was comparatively lower. According to the National Ambient  
272 Air Quality Standard of China (GB3095-2012), the daily PM<sub>2.5</sub> averages in Guangzhou can meet the  
273 Level II standard of 75 μg m<sup>-3</sup>, while exceeding the level I standard (35 μg m<sup>-3</sup>). Here, we defined  
274 PM<sub>2.5</sub> polluted days with daily mean PM<sub>2.5</sub> exceeding 35 μg m<sup>-3</sup>. As shown in Figure 5, the distribution  
275 of the corrected J<sub>NO<sub>3</sub><sup>-</sup>-HONO</sub> values in clean days were generally more dispersed and higher than those  
276 in polluted days, except in Guangzhou. The average value of J<sub>NO<sub>3</sub><sup>-</sup>-HONO</sub> in Guangzhou during air  
277 polluted conditions was slightly higher than that in clean conditions, besides much higher than the  
278 values in other cities. Because the influence of the shadowing effect has been corrected to some degree,  
279 these spatial and temporal change characteristics of J<sub>NO<sub>3</sub><sup>-</sup>-HONO</sub> in this work should be mainly related to  
280 the varied chemical and physical properties of PM<sub>2.5</sub> samples collected from different atmospheric

281 environments.

282 **Table 1.** The concentrations of PM<sub>2.5</sub>, NO<sub>3</sub><sup>-</sup>, and OC, OC/NO<sub>3</sub><sup>-</sup>, corrected J<sub>NO<sub>3</sub><sup>-</sup>-HONO</sub>, and S<sub>HONO</sub> in

283 five representative cities in China under different air conditions during the sampling period.

Site	Air condition	PM <sub>2.5</sub> (μg m <sup>-3</sup> )	NO <sub>3</sub> <sup>-</sup> (μg m <sup>-3</sup> )	OC (μg m <sup>-3</sup> )	OC/NO <sub>3</sub> <sup>-</sup>	Corrected J <sub>NO<sub>3</sub><sup>-</sup>-HONO</sub> (10 <sup>-5</sup> s <sup>-1</sup> ) <sup>a</sup>	S <sub>HONO</sub> (10 <sup>-5</sup> mol h <sup>-1</sup> m <sup>-2</sup> ) <sup>b</sup>	S <sub>HONO</sub> (ppbv h <sup>-1</sup> ) <sup>c</sup>
Beijing	Clean	19.71±8.65	3.15±2.34	3.89±2.13	2.25±3.03	2.01±2.44	0.15±0.07	0.03±0.02
	Polluted	72.56±23.78	19.71±10.72	12.62±2.18	0.87±0.62	0.61±0.30	0.38±0.11	0.09±0.02
	Whole-Min	4.32	0.08	1.07	0.32	0.21	0.04	0.01
	Whole-Max	102.64	32.90	15.95	12.82	11.06	0.57	0.13
	Whole-Mean	32.92	7.29	6.07	1.85	1.57	0.22	0.05
Changji	Clean	20.39±6.00	3.05±1.75	3.61±1.08	1.66±1.11	0.65±0.18	0.07±0.03	0.02±0.01
	Polluted	80.49±39.54	20.59±4.74	8.35±2.97	0.44±0.08	0.21±0.03	0.16±0.04	0.04±0.01
	Whole-Min	14.45	0.88	2.69	0.28	0.16	0.03 <sup>d</sup>	0.01 <sup>d</sup>
	Whole-Max	169.35	28.28	14.34	3.65	0.91	0.22	0.05
	Whole-Mean	57.37	13.84	6.53	0.91	0.39	0.13	0.03
Guangzhou	Clean	25.62±6.08	3.29±1.68	6.89±2.21	2.72±1.79	3.25±1.28	0.36±0.15	0.08±0.03
	Polluted	40.32±2.23	4.38±1.30	13.82±1.34	3.35±0.86	3.53±0.61	0.59±0.15	0.13±0.03
	Whole-Min	14.77	0.85	3.67	0.82	1.37	0.17	0.04
	Whole-Max	42.74	6.63	15.62	8.05	5.83	0.75	0.17
	Whole-Mean	29.12	3.55	8.54	2.87	3.31	0.41	0.09
Wangdu	Clean	22.16±7.66	3.29±2.59	5.36±2.38	4.79±6.46	3.80±5.10	0.20±0.09	0.04±0.02
	Polluted	83.53±30.47	18.06±12.48	23.23±9.62	1.88±1.67	1.09±0.87	0.50±0.15	0.11±0.03
	Whole-Min	10.67	0.24	2.72	0.22	0.23	0.06	0.01
	Whole-Max	173.45	60.28	63.07	22.06	19.60	0.88 <sup>e</sup>	0.20 <sup>e</sup>
	Whole-Mean	68.38	14.41	18.82	2.60	1.75	0.42	0.10
Xinxiang	Clean	23.53±5.45	4.35±1.41	5.69±2.46	1.37±0.61	1.28±0.49	0.21±0.07	0.05±0.02
	Polluted	68.98±33.43	24.87±21.5	14.63±4.41	0.87±0.45	0.62±0.35	0.40±0.12	0.09±0.03
	Whole-Min	18.32	2.37	2.33	0.30	0.19	0.09	0.02
	Whole-Max	143.10	73.47	22.06	2.02	1.96	0.59	0.13
	Whole-Mean	57.62	19.74	12.40	0.99	0.78	0.35	0.08

284 <sup>a</sup> represented the photolysis rate constant of particulate nitrate leading to HONO production after considering the

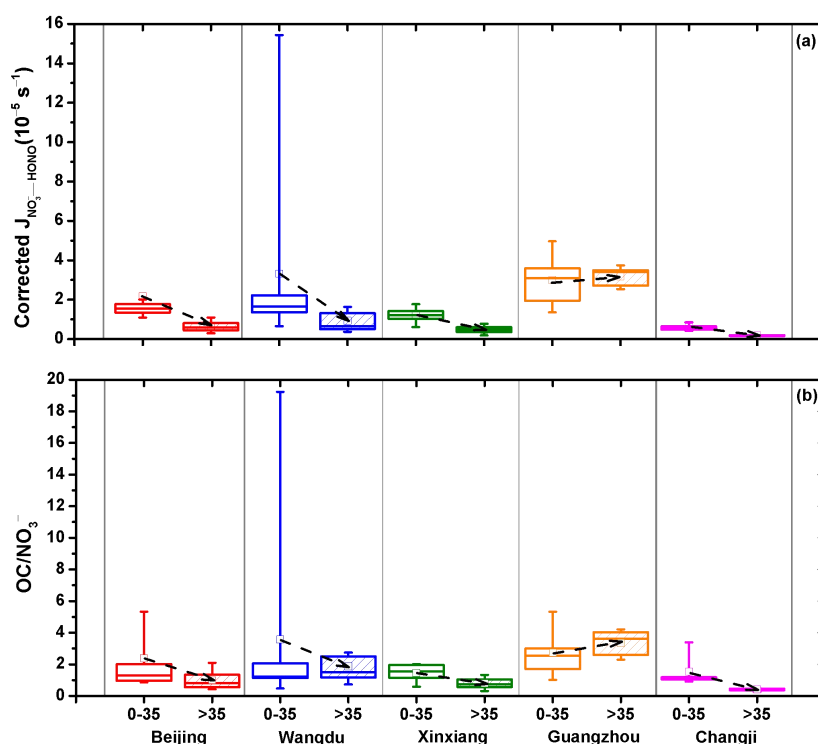
285 influence of the shadowing effect. <sup>b, c</sup> represented the noontime source strength of HONO through the photolysis of

286 particulate nitrate with the units of 10<sup>-5</sup> mol h<sup>-1</sup> m<sup>-2</sup> and ppbv h<sup>-1</sup>, respectively. <sup>d, e</sup> represented the minimum and

287 maximum values of S<sub>HONO</sub> during the observation period.

288

289



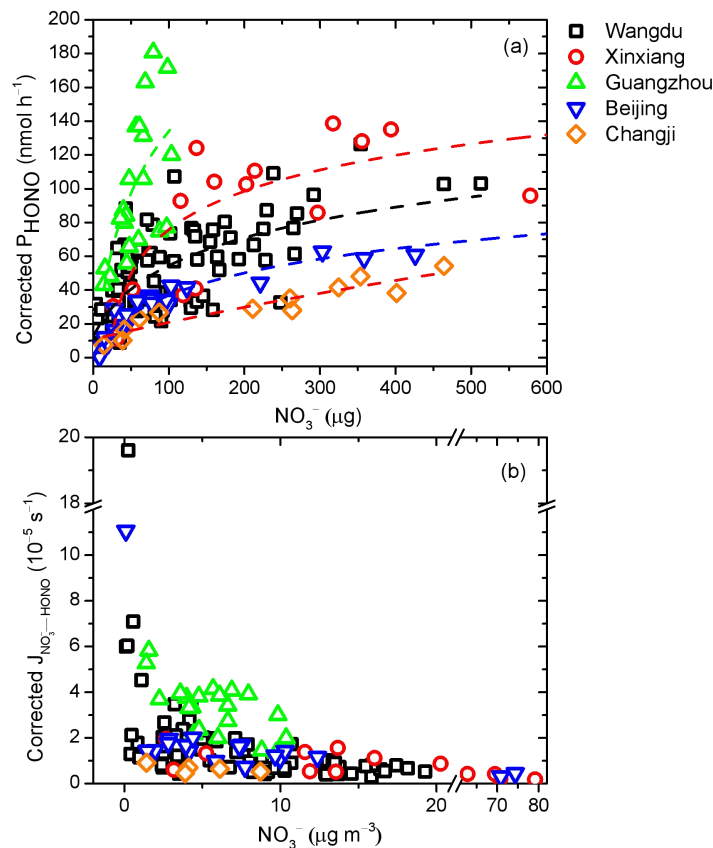
290

291 **Figure 5.** (a) Average corrected  $J_{\text{NO}_3\text{-HONO}}$ , and (b) the ratio of OC to  $\text{NO}_3^-$  under different air  
292 conditions in five representative cities. The box represents the 25th to 75th percentiles, the horizon line  
293 represents the median, the hollow square represents the mean, and the 10th and the 90th percentiles are  
294 the bottom and top whiskers, respectively.

### 295 3.3 Dominant factors controlling $J_{\text{NO}_3\text{-HONO}}$

#### 296 3.3.1 Particulate nitrate

297 As shown in Table 1, the corrected  $J_{\text{NO}_3\text{-HONO}}$  values varied with sampling periods and locations  
298 over a wide range, distributing from  $0.16 \times 10^{-5} \text{ s}^{-1}$  for the aerosol sample collected in Changji with  
299  $\text{PM}_{2.5}$  higher than  $90 \mu\text{g m}^{-3}$ , to  $19.60 \times 10^{-5} \text{ s}^{-1}$  for the aerosol sample collected in Wangdu with  $\text{PM}_{2.5}$   
300 lower than  $25 \mu\text{g m}^{-3}$ . Several factors may contribute to the discrepancy of  $J_{\text{NO}_3\text{-HONO}}$  in these  
301 different aerosol samples, such as particulate nitrate, organic matter, and aerosol acidity.



302

303 **Figure 6.** Relationships between (a) corrected  $P_{\text{HONO}}$  and particulate nitrate loading, and (b) corrected  
 304  $J_{\text{NO}_3^- - \text{HONO}}$  and particulate nitrate concentration in different sampling locations. The dash lines in (a)  
 305 were the best fits to the data for the fitting equation: the aerosol samples in Guangzhou ( $a=4.30$ ,  $b=0.06$ ,  
 306  $c=1 \times 10^{-6}$ ,  $R^2=0.42$ ), Wangdu ( $a=2.54$ ,  $b=0.11$ ,  $c=1 \times 10^{-6}$ ,  $R^2=0.50$ ), Beijing ( $a=1.51$ ,  $b=0.06$ ,  
 307  $c=1 \times 10^{-6}$ ,  $R^2=0.91$ ), Xinxiang ( $a=2.28$ ,  $b=0.06$ ,  $c=1 \times 10^{-6}$ ,  $R^2=0.47$ ), and Changji ( $a=0.58$ ,  $b=0.04$ ,  
 308  $c=1 \times 10^{-6}$ ,  $R^2=0.86$ ).

309 As shown in Figure 6, after considering the shadowing effect, the corrected  $P_{\text{HONO}}$  generally  
 310 increased along with the increased amount of particulate nitrate ( $\text{pNO}_3^-$ ,  $\mu\text{g}$ ), but still gradually slowed  
 311 down at high particulate nitrate loading, resulting in a rapid decrease in  $J_{\text{NO}_3^- - \text{HONO}}$ . For example, when  
 312  $\text{NO}_3^-$  concentration was at low level (around  $0.5 \mu\text{g m}^{-3}$ ) in Wangdu, the value of corrected  $J_{\text{NO}_3^- - \text{HONO}}$   
 313 was about 30 times higher than that at high  $\text{NO}_3^-$  concentration (around  $20 \mu\text{g m}^{-3}$ ). Previous works  
 314 found that the particulate nitrate was associated with matrix components in aerosol samples, and the  
 315 photolysis reactivity of particulate nitrate was closely associated with the surface catalysis effect (Ye et  
 316 al., 2017). In such a mechanism, the interaction between particulate nitrate and the substrate can distort  
 317 the molecular structure of nitrate and increase the absorption cross-section. The increases of  $P_{\text{HONO}}$  with  
 318  $\text{pNO}_3^-$  exposed to the light radiation can be fitted by a logarithm curve under different

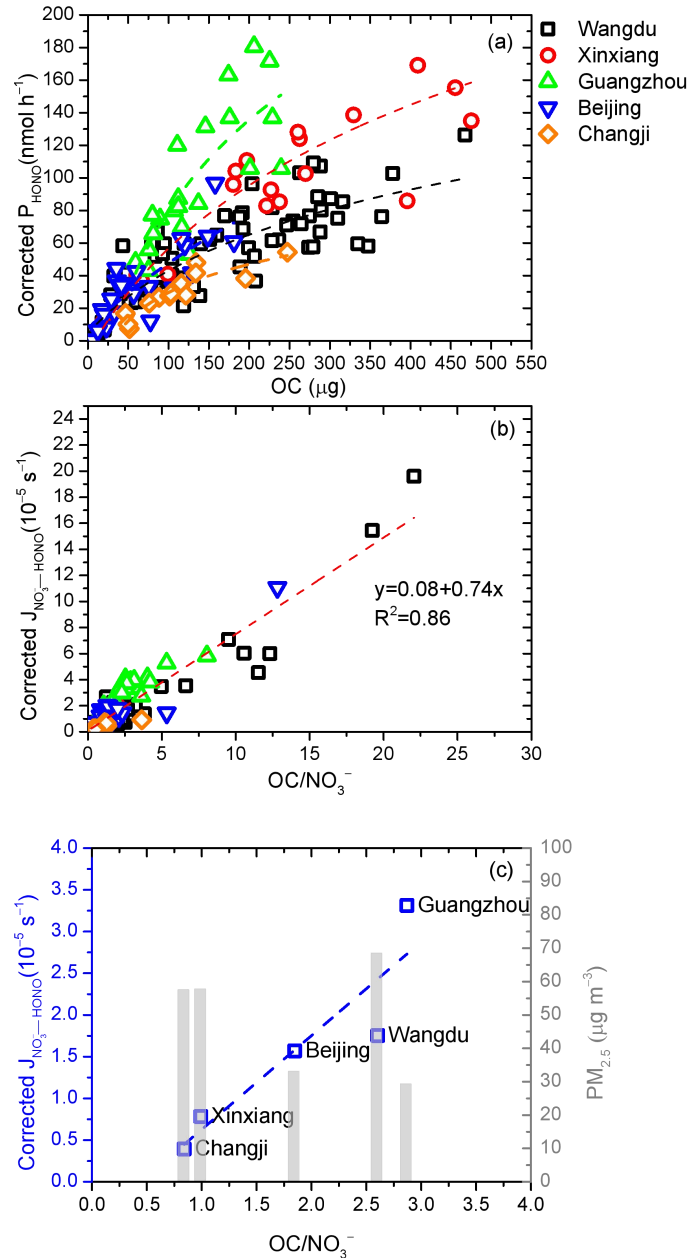
319 environment:  $P_{\text{HONO}} = \frac{a}{b} \ln(1 + b(p\text{NO}_3^-)) + c(p\text{NO}_3^-)$  (Ye et al., 2017; Ye et al., 2019). Based on this  
320 fitting equation, the corrected  $P_{\text{HONO}}$  as a function of  $p\text{NO}_3^-$  was showed in Figure 6a. Interestingly,  
321 these relationships under different sampling locations showed distinct upward trends. Ye et al. (2019)  
322 found that this ratio of a to b was related to the catalysis power of surface reactive sites and the organic  
323 matters in the matrix. The much higher ratio of a (4.30) to b (0.06) values fitted for Guangzhou than  
324 those for other cities, especially Changji (a=0.58, b=0.04), suggested extra catalytic power of organic  
325 components in addition to the surface reactive site on particulate nitrate. The large deviation of the ratio  
326 of a to b among these cities indicated the limitation of predicting  $P_{\text{HONO}}$  only based on the relationship  
327 with particulate nitrate in different atmospheric environments, and other varied aerosol chemical and  
328 physical conditions should be considered as well.

### 329 3.3.2 Organic matter

330 Organic matter was ubiquitous in the atmosphere and contributed significantly to the total aerosol  
331 mass. The selectivity of organic matter that coexisted in the aerosols was very important for the  
332 production of HONO from the photolysis of particulate nitrate (Bao et al., 2018; Ye et al., 2016a;  
333 Svoboda et al., 2013; Reeser et al., 2013; Stemmler et al., 2006; Yang et al., 2018; Beine et al., 2006;  
334 Wang et al., 2021). As shown in Figure 7a, corrected  $P_{\text{HONO}}$  generally increased as the amount of OC in  
335 aerosol samples (pOC,  $\mu\text{g}$ ) went up, while these positive correlations between  $P_{\text{HONO}}$  and pOC shown  
336 may be due to the moderate correlation between  $p\text{NO}_3^-$  and pOC ( $R^2=0.39$ , Figure S3). To eliminate  
337 the contribution from particulate nitrate, the dependence of  $J_{\text{NO}_3^--\text{HONO}}$  on the ratio of OC to  $\text{NO}_3^-$   
338 ( $\text{OC}/\text{NO}_3^-$ ) was examined:

$$339 \text{ Corrected } J_{\text{NO}_3^--\text{HONO}} = 0.74 \times (\text{OC}/\text{NO}_3^-) + 0.08 \quad (6)$$





340

341

342 **Figure 7.** Relationship between (a) corrected  $P_{\text{HONO}}$  and OC loadings, (b) corrected  $J_{\text{NO}_3-\text{HONO}}$  and  
 343  $\text{OC}/\text{NO}_3^-$ , and (c) average corrected  $J_{\text{NO}_3-\text{HONO}}$ ,  $\text{PM}_{2.5}$ , and  $\text{OC}/\text{NO}_3^-$  during the sampling period in  
 344 five representative cities.

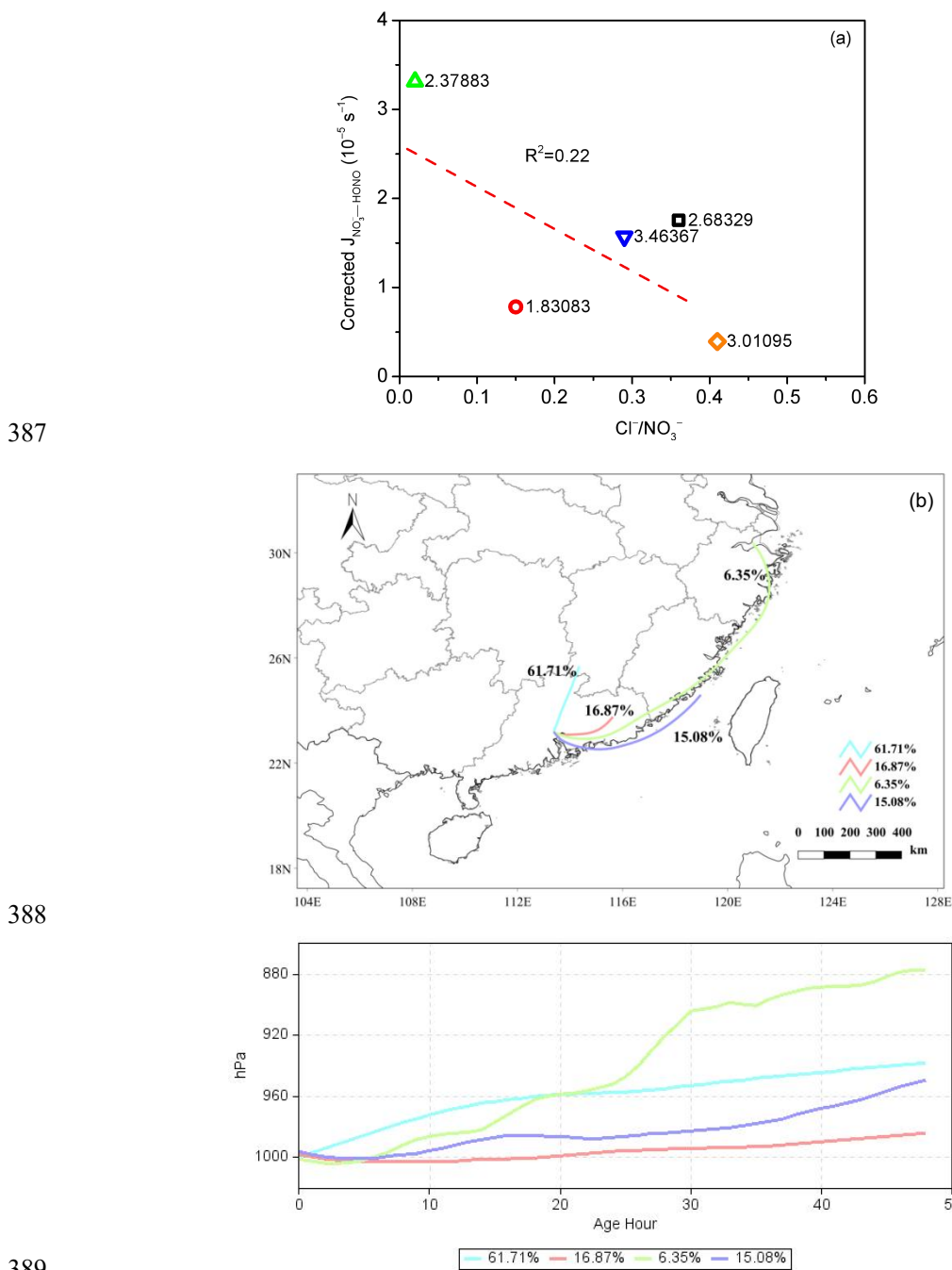
345 As shown in Figure 7b, significant linear correlation between corrected  $J_{\text{NO}_3-\text{HONO}}$  and  $\text{OC}/\text{NO}_3^-$   
 346 was found, with an  $R^2$  of 0.86. In general, high corrected  $J_{\text{NO}_3-\text{HONO}}$  values were mostly associated  
 347 with high  $\text{OC}/\text{NO}_3^-$  ratios for aerosol samples collected in the clean areas, such as Guangzhou, where  
 348 the averaged  $\text{PM}_{2.5}$  level was the lowest (Figure 7c). Low corrected  $J_{\text{NO}_3-\text{HONO}}$  values were mostly  
 349 associated with low  $\text{OC}/\text{NO}_3^-$  ratio. Generally, cities with higher  $\text{PM}_{2.5}$  levels have lower  $\text{OC}/\text{NO}_3^-$   
 350 ratios, such as Changji and Xinxiang, however, there was an exception — Wangdu, a rural site in the

351 North China Plain, where the PM<sub>2.5</sub> was high but dominated by OM mainly due to local residential coal  
352 combustion (Liu et al., 2016; Li et al., 2024; Liu et al., 2017). As shown in Figure 5b, the OC/NO<sub>3</sub><sup>-</sup>  
353 ratio in clean days was generally higher than that in polluted conditions. Interestingly, different from  
354 other cities, the OC/NO<sub>3</sub><sup>-</sup> ratio in Guangzhou increased at polluted conditions, which was consistent  
355 with the correspondingly higher corrected J<sub>NO<sub>3</sub><sup>-</sup>-HONO</sub> value. Guangzhou was located in the PRD  
356 region, and was characterized by large fractions of OM in PM<sub>2.5</sub> due to large emission of VOCs from  
357 numerous manufacturing industries and transport-related sources (Zheng et al., 2009), and the  
358 water-soluble organic carbon (WSOC) was the dominated component in the organic aerosols  
359 (WSOC/OC=0.63) (Chang et al., 2019). It's reported that organic compounds on the surface may act as  
360 photosensitizers in the photolysis of particulate nitrate (Gen et al., 2022; Handley et al., 2007; Cao et  
361 al., 2022; Wang et al., 2021). The association of particulate nitrate with organic matter may distort its  
362 molecular structure and enhance the absorption cross section, resulting in significantly enhancement in  
363 the photochemical production of HONO. The organic matter can also become hydrogen donors, and  
364 directly transfer hydrogen from organic H-donors to NO<sub>2</sub> to form HONO (Gen et al., 2022). Therefore,  
365 we suggested that the gradually increasing role of organic matter in PM<sub>2.5</sub> in China should be of great  
366 concern.

### 367 3.3.3 Other factors

368 The acidic proton may play an important role in the photochemical production of HONO  
369 and affect the release of photolysis products (Bao et al., 2018; Scharko et al., 2014). Scharko et al.  
370 (2014) found that gaseous HONO production from nitrate photolysis was the highest at the lowest  
371 aerosol acidity (pH, ~2) and decreased with pH, and reached almost zero at pH higher than 4. In this  
372 work, the estimated pH of these aerosol samples was in the range of 1.83–3.46 (the Extended Aerosol  
373 Inorganic Model, E-AIM (Shi et al., 2021; Wexler and Clegg, 2002; Clegg et al., 1998)) with detailed  
374 information provided in the Supporting Information. As shown in Figure S4, however, the correlation  
375 between pH and J<sub>NO<sub>3</sub><sup>-</sup>-HONO</sub> was weak, which indicated that pH was an important factor, but not the  
376 key one driving the spatial differences of J<sub>NO<sub>3</sub><sup>-</sup>-HONO</sub> in this work. Noting that halide ions, such as  
377 chlorine (Cl<sup>-</sup>), may lead to enhancement of surface nitrate anion and promote nitrate photolysis (Gen et  
378 al., 2022; Zhang et al., 2020a), we also plotted J<sub>NO<sub>3</sub><sup>-</sup>-HONO</sub> against the molar ratio of Cl<sup>-</sup> to NO<sub>3</sub><sup>-</sup>  
379 (Cl<sup>-</sup>/NO<sub>3</sub><sup>-</sup>) in Figure 8a. Even though Guangzhou was a southern coastal city, the sampling site in this

380 work was far away from the South China Sea (>50 km). Besides, during the observation period, the  
 381 aerosol collected in Guangzhou was more representative of inland aerosol instead of marine aerosol,  
 382 with the air parcel usually coming from inland directions (Figure 8b) and the ratio of  $\text{Cl}^-$  to  $\text{NO}_3^-$  (0.02)  
 383 much lower than that in fresh sea spray aerosol (>1.0) (Xiao et al., 2017; Pipalatkarn et al., 2014; Atzei  
 384 et al., 2019; Wang et al., 2019). Therefore, we suggested that the halide ions were not the determining  
 385 factor for the high  $J_{\text{NO}_3^--\text{HONO}}$  value in Guangzhou, and the exact role of halide ions in HONO  
 386 formation through the photolysis of particulate nitrate required further investigation.



388  
 389  
 390 **Figure 8.** (a) Relationship between the average corrected  $J_{\text{NO}_3^--\text{HONO}}$  and  $\text{Cl}^-/\text{NO}_3^-$  under different

391 sampling locations, and (b) the back trajectory cluster analysis in Guangzhou during the sampling  
392 period.

### 393 3.4 Environmental implication

394 The determined  $J_{\text{NO}_3^--\text{HONO}}$  was closely associated with the aerosol chemical and physical  
395 characteristics, especially the coexisted organic components, and distributed around the curve as  
396 expressed by Eq. (6). It's the first effort to explore the photolysis of particulate nitrate in aerosol  
397 samples collected from different typical regions of China. The enhanced formation of HONO from the  
398 photolysis of particulate nitrate can contribute significantly to the atmospheric oxidation capacity. To  
399 assess the photolysis of particulate nitrate as a HONO daytime source, the noontime source strength of  
400 HONO ( $S_{\text{HONO}}$ ) through this mechanism in the air column within the planetary boundary layer can be  
401 calculated by the following equation (Ye et al., 2017):

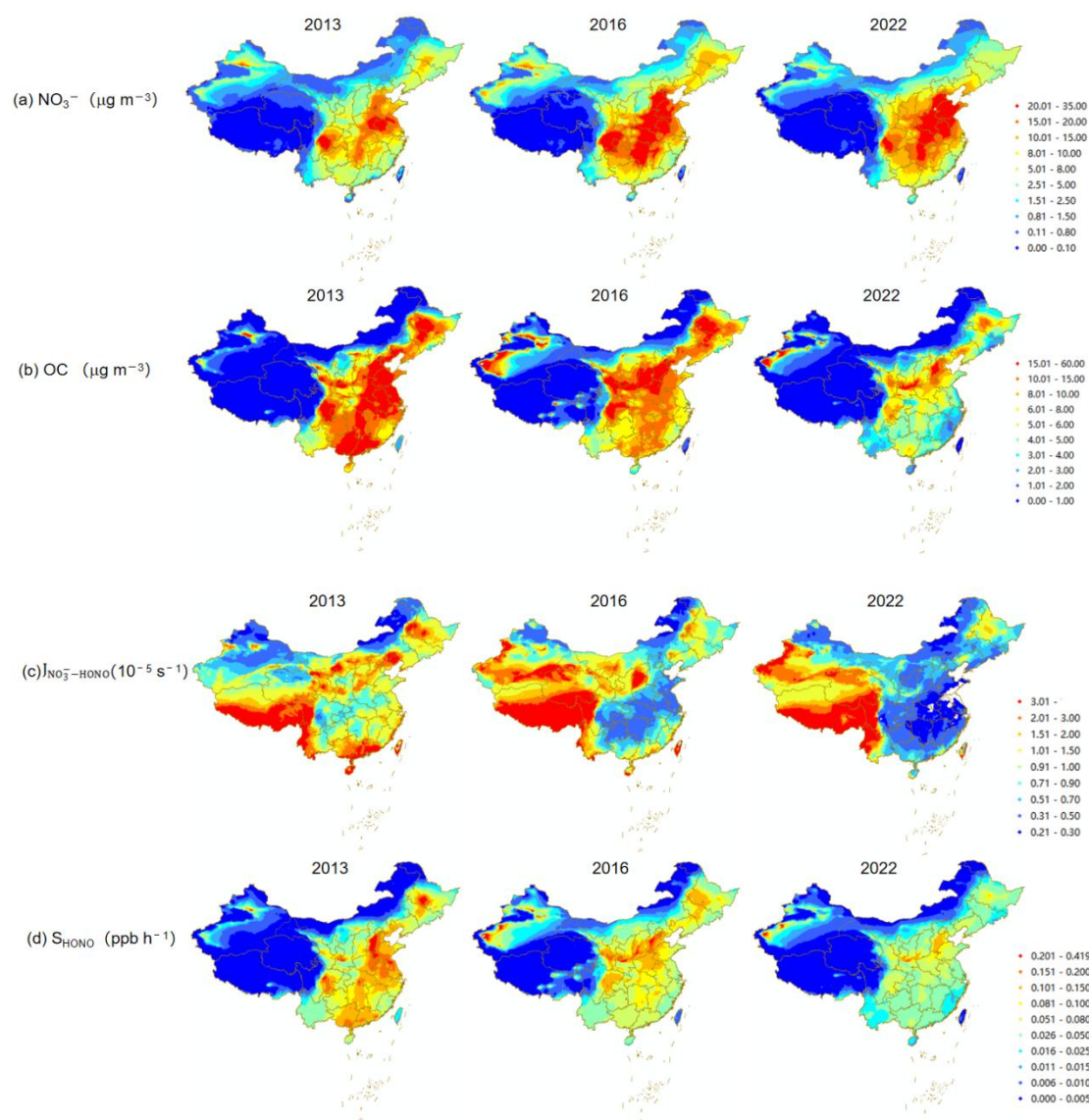
$$402 S_{\text{HONO}} (10^{-5} \text{ mol h}^{-1} \text{ m}^{-2}) = 0.67 \times \text{NO}_3^- (\mu\text{mol m}^{-3}) \times 10^{-6} \times J_{\text{NO}_3^--\text{HONO}} \times \text{BLH} \times 3600 \quad (7)$$

403 or

$$404 S_{\text{HONO}} (\text{ppbv h}^{-1}) = 0.67 \times \text{NO}_3^- (\text{ppbv}) \times J_{\text{NO}_3^--\text{HONO}} \times 3600 \quad (8)$$

405 where BLH means the boundary mixing height (m). Here, we assumed a typical BLH of 1000 m.  
406 Based on the daily measured  $\text{NO}_3^-$  and corrected  $J_{\text{NO}_3^--\text{HONO}}$  value in each city, the  $S_{\text{HONO}}$  derived from  
407 Eq. (7) or (8) during the observation period was showed in Table 1. It was found that, even though the  
408  $J_{\text{NO}_3^--\text{HONO}}$  in polluted days was much lower than that in clean days, due to the apparent higher  $\text{NO}_3^-$   
409 concentration, the corresponding  $S_{\text{HONO}}$  was about twice the average in clean days. The calculated  
410  $S_{\text{HONO}}$  ranged from  $0.03 \times 10^{-5} \text{ mol h}^{-1} \text{ m}^{-2}$  to  $0.88 \times 10^{-5} \text{ mol h}^{-1} \text{ m}^{-2}$  ( $0.01 \text{ ppbv h}^{-1}$ – $0.2 \text{ ppbv h}^{-1}$ ), with  
411 the mean value of  $0.36 \times 10^{-5} \text{ mol h}^{-1} \text{ m}^{-2}$  ( $0.08 \text{ ppbv h}^{-1}$ ), which was comparable or higher than other  
412 HONO sources (Bhattacharai et al., 2019; Wang et al., 2023b; Ye et al., 2017). For example, the soil  
413 HONO emission flux was measured in the range of  $1.81 \times 10^{-6} \text{ mol h}^{-1} \text{ m}^{-2}$ – $4.55 \times 10^{-6} \text{ mol h}^{-1} \text{ m}^{-2}$  in  
414 the soil without suffering nitrogen fertilizer (Bhattacharai et al., 2019). The mean value of  $S_{\text{HONO}}$  during  
415 the observation period was the highest in Wangdu ( $0.42 \times 10^{-5} \text{ mol h}^{-1} \text{ m}^{-2}$ ,  $0.10 \text{ ppbv h}^{-1}$ ) and  
416 Guangzhou ( $0.41 \times 10^{-5} \text{ mol h}^{-1} \text{ m}^{-2}$ ,  $0.09 \text{ ppbv h}^{-1}$ ), followed by Xinxiang ( $0.35 \times 10^{-5} \text{ mol h}^{-1} \text{ m}^{-2}$ ,  $0.08$   
417  $\text{ppbv h}^{-1}$ ), Beijing ( $0.22 \times 10^{-5} \text{ mol h}^{-1} \text{ m}^{-2}$ ,  $0.05 \text{ ppbv h}^{-1}$ ), and Changji ( $0.13 \times 10^{-5} \text{ mol h}^{-1} \text{ m}^{-2}$ ,  $0.03$   
418  $\text{ppbv h}^{-1}$ ). Even though the  $\text{PM}_{2.5}$  and  $\text{NO}_3^-$  concentration was the lowest in Guangzhou, the  $S_{\text{HONO}}$  was  
419 much higher than other cities with air pollution. It should be noted that the  $S_{\text{HONO}}$  calculated with the

420 daily changed  $\text{NO}_3^-$  and  $J_{\text{NO}_3^--\text{HONO}}$  value in this work was much lower than the value reported by Bao  
421 et al. (2018) ( $0.78 \text{ ppbv h}^{-1}$ ), which applied the average  $\text{NO}_3^-$  ( $6.64 \mu\text{g m}^{-3}$ ,  $2.62 \text{ ppbv}$ ) and the  
422  $J_{\text{NO}_3^--\text{HONO}}$  range ( $1.22 \times 10^{-5} \text{ s}^{-1}$ – $4.84 \times 10^{-4} \text{ s}^{-1}$ ) to simulate  $S_{\text{HONO}}$  ( $0.12 \text{ ppbv h}^{-1}$ – $4.57 \text{ ppbv h}^{-1}$ ). Other  
423 works, such as Fu et al. (2019) and Gu et al. (2022a), applied the mean value of  $J_{\text{NO}_3^--\text{HONO}}$  ( $8.3 \times 10^{-5}$   
424  $\text{ s}^{-1}$ ) and the observed  $\text{NO}_3^-$  concentration to calculate  $S_{\text{HONO}}$ . However, due to the significant decrease  
425 of  $J_{\text{NO}_3^--\text{HONO}}$  along with the increase of  $\text{NO}_3^-$ , the  $S_{\text{HONO}}$  calculated with mean  $\text{NO}_3^-$  or  $J_{\text{NO}_3^--\text{HONO}}$   
426 will be largely overestimated, thus directly influencing the identification of HONO sources. For  
427 example,  $J_{\text{NO}_3^--\text{HONO}}$  was the highest in Wangdu in November 23, 2023 with the value of  $19.6 \times 10^{-5} \text{ s}^{-1}$ ,  
428 while the corresponding  $\text{NO}_3^-$  concentration was low ( $0.39 \mu\text{g m}^{-3}$ ). If applying the average  $\text{NO}_3^-$   
429 concentration ( $12.53 \mu\text{g m}^{-3}$ , equivalent to  $4.53 \text{ ppbv}$ ) and the maximum  $J_{\text{NO}_3^--\text{HONO}}$  value, the  
430 determined  $S_{\text{HONO}}$  value would be  $9.56 \times 10^{-5} \text{ mol h}^{-1} \text{ m}^{-2}$  ( $2.14 \text{ ppbv h}^{-1}$ ), which was about 30 times  
431 higher than the actual result ( $0.07 \text{ ppbv h}^{-1}$ ). Therefore, we suggested to estimate  $S_{\text{HONO}}$  with the  
432 observed concentration of  $\text{NO}_3^-$  and the  $J_{\text{NO}_3^--\text{HONO}}$  value derived from the parameterization equation  
433 with  $\text{OC}/\text{NO}_3^-$ , thereby reducing the large uncertainties and improving estimations of HONO budget.



434

435

436 **Figure 9.** Spatial distributions of the daily average (a)  $\text{NO}_3^-$ , (b) OC, (c)  $J_{\text{NO}_3^--\text{HONO}}$ , and (d)  $S_{\text{HONO}}$   
 437 from November 15 to December 15 in the year of 2013, 2016, and 2022 in China. The daily average  
 438 concentrations of  $\text{NO}_3^-$  and OC were extracted from the Chinese high resolution  $\text{PM}_{2.5}$  Component  
 439 simulation concentration dataset (Kong, et al., 2024). The  $J_{\text{NO}_3^--\text{HONO}}$  and  $S_{\text{HONO}}$  estimated in this work  
 440 were derived under the same environmental conditions (RH=65 %, temperature=20 °C, and light  
 441 intensity=150  $\text{kW m}^{-2}$ ), thus were more representative of the potential of HONO production rather than  
 442 the actual value in the real ambient environment.

443 On the basis of the daily average concentrations of  $\text{NO}_3^-$  and OC extracted from the Chinese high  
 444 resolution  $\text{PM}_{2.5}$  Component simulation concentration dataset (CAQRA-aerosol,  
 445 <https://www.capdatabase.cn>, 15  $\text{km} \times 15 \text{ km}$ ) (Kong, et al., 2024), the  $J_{\text{NO}_3^--\text{HONO}}$  and  $S_{\text{HONO}}$  can be  
 446 estimated by Eq. (6) and (8), respectively. As shown in Figure 9, significant spatio-temporal change

447 characteristics of  $\text{NO}_3^-$ , OC,  $J_{\text{NO}_3^--\text{HONO}}$  and  $S_{\text{HONO}}$  were demonstrated in autumn-winter seasons from  
448 2013 to 2022 in China. The high  $J_{\text{NO}_3^--\text{HONO}}$  were concentrated in the ‘clean’ environments (e.g.,  
449 Tibetan Plateau area, South Xinjiang Basin, Yunnan-Guizhou plateaus, and Sichuan basins) and  
450 followed by those air polluted regions (e.g., NCP, Fenhe-Weihe Basin, Northeastern China, and PRD).  
451 From 2013 to 2022, with OC decreasing significantly, while  $\text{NO}_3^-$  keeping stable or even increasing,  
452  $J_{\text{NO}_3^--\text{HONO}}$  showed a downward trend in most regions. Although the  $J_{\text{NO}_3^--\text{HONO}}$  in polluted regions  
453 was comparatively lower than that in ‘clean’ environments, the higher values of  $S_{\text{HONO}}$  were mostly  
454 distributed in these polluted regions resulting from the much higher  $\text{NO}_3^-$  concentration. However, it  
455 should be noted that the photolysis of particulate nitrate contributed only a small fraction to the needed  
456 daytime HONO source in these polluted regions, such as 1.26–3.82 ppbv  $\text{h}^{-1}$  in the cities in the North  
457 China Plain (Hou et al., 2016; Wang et al., 2017; Lian et al., 2022; Li et al., 2018), 0.75 ppbv  $\text{h}^{-1}$  in the  
458 Western China (Huang et al., 2017), and 0.77–4.90 ppbv  $\text{h}^{-1}$  in Southern China (Li et al., 2012; Su et al.,  
459 2008). We noted that uncertainties still exist in our simulations. Given the paucity of filed  
460 measurements of HONO production from aerosol samples in ‘clean’ environments, the deviation of  
461  $J_{\text{NO}_3^--\text{HONO}}$  derived from the parametrization in this work may be large in these regions. Additionally,  
462 the concentrations of  $\text{NO}_3^-$  and OC extracted from the CAQRA-aerosol in ‘clean’ environments were  
463 around the mean deviation level. Therefore, more field observations and simulation experiments should  
464 be taken in these ‘clean’ regions in the future, to enrich and improve the parametric equations of  
465  $J_{\text{NO}_3^--\text{HONO}}$ , and further evaluate the contribution of nitrate photolysis to the formation of HONO in  
466 different regions in China.

#### 467 **4 Conclusions**

468 This study for the first time systematically analyzed the production of HONO from the photolysis  
469 of particulate nitrate in  $\text{PM}_{2.5}$  samples from multiple sites across China, shedding light to the  
470 contribution of this photolysis process to HONO daytime source in different environments. A total of  
471 20 pairs of comparative photochemical experiments were conducted in Wangdu to evaluate and  
472 quantify the shadowing effect. We found that the corrected  $J_{\text{NO}_3^--\text{HONO}}$  values varied with sampling  
473 periods and locations over a wide range, distributing from  $0.16 \times 10^{-5} \text{ s}^{-1}$  to  $19.60 \times 10^{-5} \text{ s}^{-1}$ . The  
474 coexisted organic components in  $\text{PM}_{2.5}$  can promote the photolysis of particulate nitrate, with higher

475  $J_{\text{NO}_3^--\text{HONO}}$  generally associated with higher  $\text{OC}/\text{NO}_3^-$  ratio. Considering the logarithmical decrease of  
476  $J_{\text{NO}_3^--\text{HONO}}$  with increased  $\text{NO}_3^-$ , we suggested that the  $S_{\text{HONO}}$  should be calculated with  $J_{\text{NO}_3^--\text{HONO}}$   
477 derived from the parameterization equation with  $\text{OC}/\text{NO}_3^-$  instead of the average value. The  
478 photolysis of particulate nitrate can become a potential daytime HONO source in southern urban cities,  
479 such as GuangZ, which was characterized by large VOCs emissions and enhanced formation of  
480 secondary particulate organic matter. Our work has provided an important reference for the research  
481 in other areas in the world with high proportion of organic components in aerosol samples, such as  
482 United States (Hass-Mitchell et al., 2024) and Europe (Bressi et al., 2021). To note, the filter samples  
483 collected in this work may not cover all representative environments in China, especially the  
484 background sites, more field observations and simulation experiments are needed in the future to better  
485 constrain the parameterization and mechanism of particulate nitrate photolysis.



486 **Data availability.** The data used in this paper can be provided upon request from the corresponding  
487 author.

488

489 **Author contributions.** **J W, B L and K Z** conceived the study and designed the experiments. **J W, B**  
490 **L, J G, C C, L W, Y Z, J L, Y Z, and X D** analyzed the data. **J W and B L** prepared the manuscript  
491 and all the coauthors helped improve the manuscript.

492

493 **Competing interests.** The authors declare that they have no conflict of interest.

494

495 **Acknowledgement.** We thank the Data Integration Program of the Major Research Plan of the  
496 National Natural Science Foundation of China (No. 92044303, <https://www.capdatabase.cn>) for  
497 making the high-resolution simulation dataset of PM<sub>2.5</sub> chemical composition in Chinese from 2013 to  
498 2020 available.

499

500 **Financial support.** This work was supported by the Central Level, Scientific Research Institutes for  
501 Basic R&D Special Fund Business, China (No. 2022YSKY-26), and the National Key Research and  
502 Development Program of China (No. 2022YFC3701100).

503 **References**

- 504 Ammann, M., Kalberer, M., Jost, D. T., Tobler, L., Rössler, E., Piguet, D., Gägeler, H. W., and  
505 Baltensperger, U.: Heterogeneous production of nitrous acid on soot in polluted air masses, *Nature*,  
506 395, 157-160, 10.1038/25965, 1998.
- 507 Andersen, S. T., Carpenter, L. J., Reed, C., Lee, J. D., Chance, R., Sherwen, T., Vaughan, A. R., Stewart,  
508 J., Edwards, P. M., Bloss, W. J., Sommariva, R., Crilley, L. R., Nott, G. J., Neves, L., Read, K.,  
509 Heard, D. E., Seakins, P. W., Whalley, L. K., Boustead, G. A., Fleming, L. T., Stone, D., and Fomba,  
510 K. W.: Extensive field evidence for the release of HONO from the photolysis of nitrate aerosols, *Sci.*  
511 *Adv.*, 9, eadd6266, doi:10.1126/sciadv.add6266, 2023.
- 512 Atzei, D., Fermo, P., Vecchi, R., Fantauzzi, M., Comite, V., Valli, G., Cocco, F., and Rossi, A.:  
513 Composition and origin of PM<sub>2.5</sub> in Mediterranean Countryside, *Environ. Pollut.*, 246, 294-302,  
514 <https://doi.org/10.1016/j.envpol.2018.12.012>, 2019.
- 515 Bao, F., Li, M., Zhang, Y., Chen, C., and Zhao, J.: Photochemical aging of Beijing urban PM<sub>2.5</sub>: HONO  
516 production, *Environ. Sci. Technol.*, 52, 6309-6316, 10.1021/acs.est.8b00538, 2018.
- 517 Bao, F., Jiang, H., Zhang, Y., Li, M., Ye, C., Wang, W., Ge, M., Chen, C., and Zhao, J.: The key role of  
518 sulfate in the photochemical renoxification on real PM<sub>2.5</sub>, *Environ. Sci. Technol.*, 54, 3121-3128,  
519 10.1021/acs.est.9b06764, 2020.
- 520 Beine, H. J., Amoroso, A., Dominé, F., King, M. D., Nardino, M., Ianniello, A., and France, J. L.:  
521 Surprisingly small HONO emissions from snow surfaces at Browning Pass, Antarctica, *Atmos.*  
522 *Chem. Phys.*, 6, 2569-2580, 10.5194/acp-6-2569-2006, 2006.
- 523 Bhattarai, H. R., Liimatainen, M., Nykänen, H., Kivimäenpää, M., Martikainen, P. J., and Maljanen, M.:  
524 Germinating wheat promotes the emission of atmospherically significant nitrous acid (HONO) gas  
525 from soils, *Soil Biol. Biochem.*, 136, 10.1016/j.soilbio.2019.06.014, 2019.
- 526 Bressi, M., Cavalli, F., Putaud, J. P., Fröhlich, R., Petit, J. E., Aas, W., Äijälä, M., Alastuey, A., Allan, J.  
527 D., Aurela, M., Berico, M., Bougiatioti, A., Bukowiecki, N., Canonaco, F., Crenn, V., Dusanter, S.,  
528 Ehn, M., Elsasser, M., Flentje, H., Graf, P., Green, D. C., Heikkinen, L., Hermann, H., Holzinger, R.,  
529 Hueglin, C., Keernik, H., Kiendler-Scharr, A., Kubelová, L., Lunder, C., Maasikmets, M., Makeš, O.,  
530 Malaguti, A., Mihalopoulos, N., Nicolas, J. B., O'Dowd, C., Ovadnevaite, J., Petralia, E., Poulain, L.,  
531 Priestman, M., Riffault, V., Ripoll, A., Schlag, P., Schwarz, J., Sciare, J., Slowik, J., Sosedova, Y.,

532 Stavroulas, I., Teinmaa, E., Via, M., Vodička, P., Williams, P. I., Wiedensohler, A., Young, D. E.,  
533 Zhang, S., Favez, O., Minguillón, M. C., and Prevot, A. S. H.: A European aerosol phenomenology -  
534 7: High-time resolution chemical characteristics of submicron particulate matter across Europe,  
535 *Atmos. Environ.*: X, 10, 10.1016/j.aeaoa.2021.100108, 2021.

536 Cao, Y., Ma, Q., Chu, B., and He, H.: Homogeneous and heterogeneous photolysis of nitrate in the  
537 atmosphere: state of the science, current research needs, and future prospects, *Front. Env. Sci. Eng.*,  
538 17, 10.1007/s11783-023-1648-6, 2022.

539 Chang, D., Wang, Z., Guo, J., Li, T., Liang, Y., Kang, L., Xia, M., Wang, Y., Yu, C., Yun, H., Yue, D.,  
540 and Wang, T.: Characterization of organic aerosols and their precursors in southern China during a  
541 severe haze episode in January 2017, *Sci. Total. Environ.*, 691, 101-111,  
542 10.1016/j.scitotenv.2019.07.123, 2019.

543 Cheng, C., Yang, S., Yuan, B., Pei, C., Zhou, Z., Mao, L., Liu, S., Chen, D., Cheng, X., Li, M., Shao,  
544 M., and Zhou, Z.: The significant contribution of nitrate to a severe haze event in the winter of  
545 Guangzhou, China, *Sci. Total. Environ.*, 909, 168582, 10.1016/j.scitotenv.2023.168582, 2024.

546 Clegg, S. L., Brimblecombe, P., and Wexler, A. S.: Thermodynamic Model of the System  
547  $\text{H}^+ - \text{NH}_4^+ - \text{Na}^+ - \text{SO}_4^{2-} - \text{NO}_3^- - \text{Cl}^- - \text{H}_2\text{O}$  at 298.15 K, *J. Phy. Chem. A*, 102, 2155-2171,  
548 10.1021/jp973043j, 1998.

549 Finlayson-Pitts, B. J. a. P. J., J. N.: *Chemistry of the upper and lower atmosphere: theory, experiments,*  
550 *and applications*, Academic Press, San Diego, CA, xxii+969 pp., ISBN 0-12-257060-x, 2000.

551 Fu, X., Wang, T., Zhang, L., Li, Q., Wang, Z., Xia, M., Yun, H., Wang, W., Yu, C., Yue, D., Zhou, Y.,  
552 Zheng, J., and Han, R.: The significant contribution of HONO to secondary pollutants during a  
553 severe winter pollution event in southern China, *Atmos. Chem. Phys.*, 19, 1-14,  
554 10.5194/acp-19-1-2019, 2019.

555 Gelencsér, A., Hoffer, A., Kiss, G., Tombácz, E., Kurdi, R., and Bencze, L.: In-situ formation of  
556 light-absorbing organic matter in cloud water, *J. Atmos. Chem.*, 45, 25-33,  
557 10.1023/A:1024060428172, 2003.

558 Gen, M., Liang, Z., Zhang, R., Go Mabato, B. R., and Chan, C. K.: Particulate nitrate photolysis in the  
559 atmosphere, *Environ. Sci.-Atmos.*, 2, 111-127, 10.1039/d1ea00087j, 2022.

560 Gu, R., Shen, H., Xue, L., Wang, T., Gao, J., Li, H., Liang, Y., Xia, M., Yu, C., Liu, Y., and Wang, W.:  
561 Investigating the sources of atmospheric nitrous acid (HONO) in the megacity of Beijing, China, *Sci.*

562 Total Environ., 812, 10.1016/j.scitotenv.2021.152270, 2022a.

563 Gu, R., Wang, W., Peng, X., Xia, M., Zhao, M., Zhang, Y., Wang, Y., Liu, Y., Shen, H., Xue, L., Wang,  
564 T., and Wang, W.: Nitrous acid in the polluted coastal atmosphere of the South China Sea: Ship  
565 emissions, budgets, and impacts, *Sci. Total. Environ.*, 153692, 10.1016/j.scitotenv.2022.153692,  
566 2022b.

567 Handley, S. R., Clifford, D., and Donaldson, D. J.: Photochemical loss of nitric acid on organic films: a  
568 possible recycling mechanism for NO<sub>x</sub>, *Environ. Sci. Technol.*, 41, 3898-3903, 10.1021/es062044z,  
569 2007.

570 Hass-Mitchell, T., Joo, T., Rogers, M., Nault, B. A., Soong, C., Tran, M., Seo, M., Machesky, J. E.,  
571 Canagaratna, M., Roscioli, J., Claflin, M. S., Lerner, B. M., Blomdahl, D. C., Misztal, P. K., Ng, N.  
572 L., Dillner, A. M., Bahreini, R., Russell, A., Krechmer, J. E., Lambe, A., and Gentner, D. R.:  
573 Increasing contributions of temperature-dependent oxygenated organic aerosol to summertime  
574 particulate matter in New York City, *ACS Environ. Sci. Technol. Air*, 1, 113-128,  
575 10.1021/acsestair.3c00037, 2024.

576 Hou, S., Tong, S., Ge, M., and An, J.: Comparison of atmospheric nitrous acid during severe haze and  
577 clean periods in Beijing, China, *Atmos. Environ.*, 124, 199-206, 10.1016/j.atmosenv.2015.06.023,  
578 2016.

579 Huang, R., Yang, L., Cao, J., Wang, Q., Tie, X., Ho, K., Shen, Z., Zhang, R., Li, G., Zhu, C., Zhang, N.,  
580 Dai, W., Zhou, J., Liu, S., Chen, Y., Chen, J., and O'Dowd, C. D.: Concentration and sources of  
581 atmospheric nitrous acid (HONO) at an urban site in Western China, *Sci. Total Environ.*, 593-594,  
582 165-172, <https://doi.org/10.1016/j.scitotenv.2017.02.166>, 2017.

583 Kim, M. and Or, D.: Microscale pH variations during drying of soils and desert biocrusts affect HONO  
584 and NH<sub>3</sub> emissions, *Nat. Commun.*, 10, 3944, 10.1038/s41467-019-11956-6, 2019.

585 Kong, L., Tang, X., Zhu, J., Wang, Z., Liu, B., Zhu, Y., Zhu, L., Chen, D., Hu, K., Wu, H., Wu, Q.,  
586 Shen, J., Sun, Y., Liu, Z., Xin, J., Ji, D., and Zheng, M.: High-resolution simulation dataset of hourly  
587 PM<sub>2.5</sub> chemical composition in China (CAQRA-aerosol) from 2013 to 2020, *Adv. Atmos. Sci.*, 41,  
588 1-16, 10.1007/s00376-024-4046-5, 2024.

589 Kurtenbach, R., Becker, K. H., Gomes, J. A. G., Kleffmann, J., Lörzer, J. C., Spittler, M., Wiesen, P.,  
590 Ackermann, R., Geyer, A., and Platt, U.: Investigations of emissions and heterogeneous formation of  
591 HONO in a road traffic tunnel, *Atmos. Environ.*, 35, 3385-3394,

592 [https://doi.org/10.1016/S1352-2310\(01\)00138-8](https://doi.org/10.1016/S1352-2310(01)00138-8), 2001.

593 Lee, J. D., Whalley, L. K., Heard, D. E., Stone, D., Dunmore, R. E., Hamilton, J. F., Young, D. E.,  
594 Allan, J. D., Laufs, S., and Kleffmann, J.: Detailed budget analysis of HONO in central London  
595 reveals a missing daytime source, *Atmos. Chem. Phys.*, 16, 2747-2764, 10.5194/acp-16-2747-2016,  
596 2016.

597 Li, D., Xue, L., Wen, L., Wang, X., Chen, T., Mellouki, A., Chen, J., and Wang, W.: Characteristics and  
598 sources of nitrous acid in an urban atmosphere of northern China: Results from 1-yr continuous  
599 observations, *Atmos. Environ.*, 182, 296-306, <https://doi.org/10.1016/j.atmosenv.2018.03.033>, 2018.

600 Li, W., Tong, S., Cao, J., Su, H., Zhang, W., Wang, L., Jia, C., Zhang, X., Wang, Z., Chen, M., and Ge,  
601 M.: Comparative observation of atmospheric nitrous acid (HONO) in Xi'an and Xianyang located in  
602 the GuanZhong basin of western China, *Environ. Pollut.*, 289, 117679,  
603 10.1016/j.envpol.2021.117679, 2021.

604 Li, X., Brauers, T., Häsel, R., Bohn, B., Fuchs, H., Hofzumahaus, A., Holland, F., Lou, S., Lu, K. D.,  
605 Rohrer, F., Hu, M., Zeng, L. M., Zhang, Y. H., Garland, R. M., Su, H., Nowak, A., Wiedensohler, A.,  
606 Takegawa, N., Shao, M., and Wahner, A.: Exploring the atmospheric chemistry of nitrous acid  
607 (HONO) at a rural site in Southern China, *Atmos. Chem. Phys.*, 12, 1497-1513,  
608 10.5194/acp-12-1497-2012, 2012.

609 Li, Y., An, J., Min, M., Zhang, W., Wang, F., and Xie, P.: Impacts of HONO sources on the air quality  
610 in Beijing, Tianjin and Hebei Province of China, *Atmos. Environ.*, 45, 4735-4744,  
611 <https://doi.org/10.1016/j.atmosenv.2011.04.086>, 2011.

612 Li, Z., Ren, Z., Liu, C., Ning, Z., Liu, J., Liu, J., Zhai, Z., Ma, X., Chen, L., Zhang, Y., Bai, L., and  
613 Kong, S.: Heterogeneous variations in wintertime PM<sub>2.5</sub> sources, compositions and exposure risks at  
614 urban/suburban rural/remote rural areas in the post COVID-19/Clean-Heating period, *Atmos.*  
615 *Environ.*, 326, 120463, <https://doi.org/10.1016/j.atmosenv.2024.120463>, 2024.

616 Lian, C., Wang, W., Chen, Y., Zhang, Y., Zhang, J., Liu, Y., Fan, X., Li, C., Zhan, J., Lin, Z., Hua, C.,  
617 Zhang, W., Liu, M., Li, J., Wang, X., An, J., and Ge, M.: Long-term winter observation of nitrous  
618 acid in the urban area of Beijing, *J. Environ. Sci. (China)*, 114, 334-342, 10.1016/j.jes.2021.09.010,  
619 2022.

620 Liang, Y., Zha, Q., Wang, W., Cui, L., Lui, K. H., Ho, K. F., Wang, Z., Lee, S., and Wang, T.: Revisiting  
621 nitrous acid (HONO) emission from on-road vehicles: A tunnel study with a mixed fleet, *J. Air Waste*

622 Manage., 67, 797-805, 10.1080/10962247.2017.1293573, 2017.

623 Liao, S., Zhang, J., Yu, F., Zhu, M., Liu, J., Ou, J., Dong, H., Sha, Q., Zhong, Z., Xie, Y., Luo, H.,  
624 Zhang, L., and Zheng, J.: High gaseous nitrous acid (HONO) emissions from light-duty diesel  
625 vehicles, Environ. Sci. Technol., 55, 200-208, 10.1021/acs.est.0c05599, 2021.

626 Liu, P., Zhang, C., Mu, Y., Liu, C., Xue, C., Ye, C., Liu, J., Zhang, Y., and Zhang, H.: The possible  
627 contribution of the periodic emissions from farmers' activities in the North China Plain to  
628 atmospheric water-soluble ions in Beijing, Atmos. Chem. Phys., 16, 10097-10109,  
629 10.5194/acp-16-10097-2016, 2016.

630 Liu, P., Zhang, C., Xue, C., Mu, Y., Liu, J., Zhang, Y., Tian, D., Ye, C., Zhang, H., and Guan, J.: The  
631 contribution of residential coal combustion to atmospheric PM<sub>2.5</sub> in northern China during winter,  
632 Atmos. Chem. Phys., 17, 11503-11520, 10.5194/acp-17-11503-2017, 2017.

633 Liu, Y., Lu, K., Li, X., Dong, H., Tan, Z., Wang, H., Zou, Q., Wu, Y., Zeng, L., Hu, M., Min, K.-E.,  
634 Kecorius, S., Wiedensohler, A., and Zhang, Y.: A comprehensive model test of the HONO sources  
635 constrained to field measurements at rural North China Plain, Environ. Sci. Technol., 53, 3517-3525,  
636 10.1021/acs.est.8b06367, 2019.

637 Melissa A, D.: Soil surface acidity plays a determining role in the atmospheric-terrestrial exchange of  
638 nitrous acid, Proc. Natl. Acad. Sci. U. S. A., 52, 18472-18477, 10.1073/pnas.1418545112, 2014.

639 Monge, M. E., D'Anna, B., Mazri, L., Giroir-Fendler, A., Ammann, M., Donaldson, D. J., and George,  
640 C.: Light changes the atmospheric reactivity of soot, Proc. Natl. Acad. Sci. U. S. A., 107, 6605-6609,  
641 10.1073/pnas.0908341107, 2010.

642 Mora Garcia, S. L., Pandit, S., Navea, J. G., and Grassian, V. H.: Nitrous acid (HONO) formation from  
643 the irradiation of aqueous nitrate solutions in the presence of marine chromophoric dissolved organic  
644 matter: comparison to other organic photosensitizers, ACS Earth Space Chem., 5, 3056-3064,  
645 10.1021/acsearthspacechem.1c00292, 2021.

646 Oswald, R., Behrendt, T., Ermel, M., Wu, D., Su, H., Cheng, Y., Breuninger, C., Moravek, A., Mougín,  
647 E., Delon, C., Loubet, B., Pommerening-Roser, A., Sorgel, M., Poschl, U., Hoffmann, T., Andreae,  
648 M. O., Meixner, F. X., and Trebs, I.: HONO emissions from soil bacteria as a major source of  
649 atmospheric reactive nitrogen, Science, 341, 1233-1235, 10.1126/science.1242266, 2013.

650 Pipalatkhar, P., Khaparde, V. V., Gajghate, D. G., and Bawase, M. A.: Source apportionment of PM<sub>2.5</sub>  
651 using a CMB model for a centrally located Indian city, Aerosol Air Qual. Res., 14, 1089-1099,

652 10.4209/aaqr.2013.04.0130, 2014.

653 Reeser, D. I., Kwamena, N.-O. A., and Donaldson, D. J.: Effect of organic coatings on gas-phase  
654 nitrogen dioxide production from aqueous nitrate photolysis, *J. Phys. Chem. C*, 117, 22260-22267,  
655 10.1021/jp401545k, 2013.

656 Ren, X., Harder, H., Martinez, M., Leshner, R. L., Oligier, A., Simpas, J. B., Brune, W. H., Schwab, J. J.,  
657 Demerjian, K. L., He, Y., Zhou, X., and Gao, H.: OH and HO<sub>2</sub> Chemistry in the urban atmosphere of  
658 New York City, *Atmos. Environ.*, 37, 3639-3651, [https://doi.org/10.1016/S1352-2310\(03\)00459-X](https://doi.org/10.1016/S1352-2310(03)00459-X),  
659 2003.

660 Romer, P. S., Wooldridge, P. J., Crouse, J. D., Kim, M. J., Wennberg, P. O., Dibb, J. E., Scheuer, E.,  
661 Blake, D. R., Meinardi, S., Brosius, A. L., Thames, A. B., Miller, D. O., Brune, W. H., Hall, S. R.,  
662 Ryerson, T. B., and Cohen, R. C.: Constraints on aerosol nitrate photolysis as a potential source of  
663 HONO and NO<sub>x</sub>, *Environ. Sci. Technol.*, 52, 13738-13746, 10.1021/acs.est.8b03861, 2018.

664 Scharko, N. K., Berke, A. E., and Raff, J. D.: Release of nitrous acid and nitrogen dioxide from nitrate  
665 photolysis in acidic aqueous solutions, *Environ. Sci. Technol.*, 48, 11991-12001, 10.1021/es503088x,  
666 2014.

667 Shi, Q., Tao, Y., Krechmer, J. E., Heald, C. L., Murphy, J. G., Kroll, J. H., and Ye, Q.: Laboratory  
668 investigation of renoxification from the photolysis of inorganic particulate nitrate, *Environ. Sci.*  
669 *Technol.*, 55, 854-861, 10.1021/acs.est.0c06049, 2021.

670 Slater, E. J., Whalley, L. K., Woodward-Massey, R., Ye, C., Lee, J. D., Squires, F., Hopkins, J. R.,  
671 Dunmore, R. E., Shaw, M., Hamilton, J. F., Lewis, A. C., Crilley, L. R., Kramer, L., Bloss, W., Vu, T.,  
672 Sun, Y., Xu, W., Yue, S., Ren, L., Acton, W. J. F., Hewitt, C. N., Wang, X., Fu, P., and Heard, D. E.:  
673 Elevated levels of OH observed in haze events during wintertime in central Beijing, *Atmos. Chem.*  
674 *Phys.*, 20, 14847-14871, 10.5194/acp-20-14847-2020, 2020.

675 Stemmler, K., Ammann, M., Donders, C., Kleffmann, J., and George, C.: Photosensitized reduction of  
676 nitrogen dioxide on humic acid as a source of nitrous acid, *Nature*, 440, 195-198,  
677 10.1038/nature04603, 2006.

678 Su, H., Cheng, Y. F., Shao, M., Gao, D. F., Yu, Z. Y., Zeng, L. M., Slanina, J., Zhang, Y. H., and  
679 Wiedensohler, A.: Nitrous acid (HONO) and its daytime sources at a rural site during the 2004  
680 PRIDE-PRD experiment in China, *J. Geophys. Res. Atmos.*, 113, 10.1029/2007jd009060, 2008.

681 Su, H., Cheng, Y., Oswald, R., Behrendt, T., Trebs, I., Meixner, F. X., Andreae, M. O., Cheng, P., Zhang,

682 Y., and Poschl, U.: Soil nitrite as a source of atmospheric HONO and OH radicals, *Science*, 333,  
683 1616-1618, 10.1126/science.1207687, 2011.

684 Svoboda, O., Kubelová, L., and Slavíček, P.: Enabling forbidden processes: quantum and solvation  
685 enhancement of nitrate anion UV absorption, *J. Phys. Chem. A*, 117, 12868-12877,  
686 10.1021/jp4098777, 2013.

687 Villena, G., Wiesen, P., Cantrell, C. A., Flocke, F., Fried, A., Hall, S. R., Hornbrook, R. S., Knapp, D.,  
688 Kosciuch, E., Mauldin, R. L., McGrath, J. A., Montzka, D., Richter, D., Ullmann, K., Walega, J.,  
689 Weibring, P., Weinheimer, A., Staebler, R. M., Liao, J., Huey, L. G., and Kleffmann, J.: Nitrous acid  
690 (HONO) during polar spring in Barrow, Alaska: A net source of OH radicals?, *J. Geophys. Res.*, 116,  
691 10.1029/2011jd016643, 2011.

692 Wang, H., Ding, J., Xu, J., Wen, J., Han, J., Wang, K., Shi, G., Feng, Y., Ivey, C. E., Wang, Y., Nenes,  
693 A., Zhao, Q., and Russell, A. G.: Aerosols in an arid environment: The role of aerosol water content,  
694 particulate acidity, precursors, and relative humidity on secondary inorganic aerosols, *Sci. Total  
695 Environ.*, 646, 564-572, <https://doi.org/10.1016/j.scitotenv.2018.07.321>, 2019.

696 Wang, J., Zhang, X., Guo, J., Wang, Z., and Zhang, M.: Observation of nitrous acid (HONO) in Beijing,  
697 China: Seasonal variation, nocturnal formation and daytime budget, *Sci. Total Environ.*, 587-588,  
698 350-359, 10.1016/j.scitotenv.2017.02.159, 2017.

699 Wang, J., Gao, J., Che, F., Wang, Y., Lin, P., and Zhang, Y.: Decade-long trends in chemical component  
700 properties of PM<sub>2.5</sub> in Beijing, China (2011-2020), *Sci. Total Environ.*, 832, 154664,  
701 10.1016/j.scitotenv.2022.154664, 2022a.

702 Wang, J., Gao, J., Che, F., Wang, Y., Lin, P., and Zhang, Y.: Dramatic changes in aerosol composition  
703 during the 2016-2020 heating seasons in Beijing-Tianjin-Hebei region and its surrounding areas: The  
704 role of primary pollutants and secondary aerosol formation, *Sci. Total. Environ.*, 849, 157621,  
705 10.1016/j.scitotenv.2022.157621, 2022b.

706 Wang, J., Zhang, Y., Zhang, C., Wang, Y., Zhou, J., Whalley, L. K., Slater, E. J., Dyson, J. E., Xu, W.,  
707 Cheng, P., Han, B., Wang, L., Yu, X., Wang, Y., Woodward-Massey, R., Lin, W., Zhao, W., Zeng, L.,  
708 Ma, Z., Heard, D. E., and Ye, C.: Validating HONO as an intermediate tracer of the external cycling  
709 of reactive nitrogen in the background atmosphere, *Environ. Sci. Technol.*, 57, 5474-5484,  
710 10.1021/acs.est.2c06731, 2023a.

711 Wang, Y., Fu, X., Wang, T., Ma, J., Gao, H., Wang, X., and Pu, W.: Large contribution of nitrous acid to



712 soil-emitted reactive oxidized nitrogen and its effect on air quality, *Environ. Sci. Technol.*, 57,  
713 3516-3526, 10.1021/acs.est.2c07793, 2023b.

714 Wang, Y., Xiao, S., Zhang, Y., Chang, H., Martin, R. V., Van Donkelaar, A., Gaskins, A., Liu, Y., Liu, P.,  
715 and Shi, L.: Long-term exposure to PM<sub>2.5</sub> major components and mortality in the southeastern  
716 United States, *Environ. Int.*, 158, 106969, 10.1016/j.envint.2021.106969, 2022c.

717 Wang, Y., Huang, D. D., Huang, W., Liu, B., Chen, Q., Huang, R., Gen, M., Mabato, B. R. G., Chan, C.  
718 K., Li, X., Hao, T., Tan, Y., Hoi, K. I., Mok, K. M., and Li, Y. J.: Enhanced nitrite production from  
719 the aqueous photolysis of nitrate in the presence of vanillic acid and implications for the roles of  
720 light-absorbing organics, *Environ. Sci. Technol.*, 55, 15694-15704, 10.1021/acs.est.1c04642, 2021.

721 Wang, Z., Zhang, D., Liu, B., Li, Y., Chen, T., Sun, F., Yang, D., Liang, Y., Chang, M., Yang, L., and  
722 Lin, A.: Analysis of chemical characteristics of PM<sub>2.5</sub> in Beijing over a 1-year period, *J. Atmos.*  
723 *Chem.*, 73, 407-425, 10.1007/s10874-016-9334-8, 2016.

724 Wexler, A. S. and Clegg, S. L.: Atmospheric aerosol models for systems including the ions H<sup>+</sup>, NH<sub>4</sub><sup>+</sup>,  
725 Na<sup>+</sup>, SO<sub>4</sub><sup>2-</sup>, NO<sub>3</sub><sup>-</sup>, Cl<sup>-</sup>, Br<sup>-</sup>, and H<sub>2</sub>O, *J. Geophys. Res. Atmos.*, 107, ACH 14-1-ACH 14-14,  
726 <https://doi.org/10.1029/2001JD000451>, 2002.

727 Xiao, H. W., Xiao, H. Y., Luo, L., Shen, C. Y., Long, A. M., Chen, L., Long, Z. H., and Li, D. N.:  
728 Atmospheric aerosol compositions over the South China Sea: temporal variability and source  
729 apportionment, *Atmos. Chem. Phys.*, 17, 3199-3214, 10.5194/acp-17-3199-2017, 2017.

730 Yang, W., Han, C., Yang, H., and Xue, X.: Significant HONO formation by the photolysis of nitrates in  
731 the presence of humic acids, *Environ. Pollut.*, 243, 679-686, 10.1016/j.envpol.2018.09.039, 2018.

732 Ye, C., Gao, H., Zhang, N., and Zhou, X.: Photolysis of nitric acid and nitrate on natural and artificial  
733 surfaces, *Environ. Sci. Technol.*, 50, 3530-3536, 10.1021/acs.est.5b05032, 2016a.

734 Ye, C., Zhang, N., Gao, H., and Zhou, X.: Photolysis of particulate nitrate as a source of HONO and  
735 NO<sub>x</sub>, *Environ. Sci. Technol.*, 51, 6849-6856, 10.1021/acs.est.7b00387, 2017.

736 Ye, C., Zhang, N., Gao, H., and Zhou, X.: Matrix effect on surface-catalyzed photolysis of nitric acid,  
737 *Sci. Rep.*, 9, 4351, 10.1038/s41598-018-37973-x, 2019.

738 Ye, C., Zhou, X., Pu, D., Stutz, J., Festa, J., Spolaor, M., Tsai, C., Cantrell, C., Mauldin, R. L., Campos,  
739 T., Weinheimer, A., Hornbrook, R. S., Apel, E. C., Guenther, A., Kaser, L., Yuan, B., Karl, T.,  
740 Haggerty, J., Hall, S., Ullmann, K., Smith, J. N., Ortega, J., and Knote, C.: Rapid cycling of reactive  
741 nitrogen in the marine boundary layer, *Nature*, 532, 489-491, 10.1038/nature17195, 2016b.

742 Zhang, L., Wang, T., Zhang, Q., Zheng, J., Xu, Z., and Lv, M.: Potential sources of nitrous acid (HONO)  
743 and their impacts on ozone: A WRF-Chem study in a polluted subtropical region, *J. Geophys. Res.*  
744 *Atmos.*, 121, 3645-3662, <https://doi.org/10.1002/2015JD024468>, 2016.

745 Zhang, R., Gen, M., Huang, D., Li, Y., and Chan, C. K.: Enhanced sulfate production by nitrate  
746 photolysis in the presence of halide ions in atmospheric particles, *Environ. Sci. Technol.*, 54,  
747 3831-3839, 10.1021/acs.est.9b06445, 2020a.

748 Zhang, W., Tong, S., Jia, C., Wang, L., Liu, B., Tang, G., Ji, D., Hu, B., Liu, Z., Li, W., Wang, Z., Liu,  
749 Y., Wang, Y., and Ge, M.: Different HONO sources for three layers at the urban area of Beijing,  
750 *Environ. Sci. Technol.*, 54, 12870-12880, 10.1021/acs.est.0c02146, 2020b.

751 Zheng, J., Shao, M., Che, W., Zhang, L., Zhong, L., Zhang, Y., and Streets, D.: Speciated VOC  
752 emission inventory and spatial patterns of ozone formation potential in the Pearl River Delta, China,  
753 *Environ. Sci. Technol.*, 43, 8580-8586, 10.1021/es901688e, 2009.

754 Zhou, X., Gao, H., He, Y., Huang, G., Bertman, S. B., Civerolo, K., and Schwab, J.: Nitric acid  
755 photolysis on surfaces in low-NO<sub>x</sub> environments: Significant atmospheric implications, *Geophys.*  
756 *Res. Let.*, 30, <https://doi.org/10.1029/2003GL018620>, 2003.

757 Zhou, X., Zhang, N., TerAvest, M., Tang, D., Hou, J., Bertman, S., Alaghmand, M., Shepson, P. B.,  
758 Carroll, M. A., Griffith, S., Dusanter, S., and Stevens, P. S.: Nitric acid photolysis on forest canopy  
759 surface as a source for tropospheric nitrous acid, *Nat. Geosci.*, 4, 440-443, 10.1038/ngeo1164, 2011.